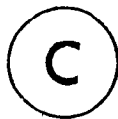


THE 0.230 MILLISECOND ISOMER IN ^{146}Eu

by



KEVIN LENESTOUR, B.Sc.

A Thesis

Submitted to the School of Graduate Studies

in Partial Fulfilment of the Requirements

for the degree

Master of Science

McMaster University

October 1980

MASTER OF SCIENCE (1980)
(Physics)

McMASTER UNIVERSITY
Hamilton, Ontario

TITLE: The 0.230 Millisecond Isomer in ^{146}Eu

AUTHOR: Kevin LeNestour, B.Sc., McMaster University

SUPERVISOR: Dr. R. G. Summers-Gill

NO. OF PAGES: x, 61

ABSTRACT

The levels associated with the decay of the 0.230 ms isomer in ^{146}Eu were populated by the $(^7\text{Li},3n)$ reaction on ^{142}Nd using a 33 Mev beam of ^7Li ions. A decay scheme has been proposed for this isomer based on the study of the in-beam and pulsed beam conversion electron, and gamma ray singles spectra. The assignment of spins and parities was based on the multipolarities of the 274.9, 293.9, 358.2 and 377.0 keV transitions determined by conversion coefficient measurements, and the assumed 9^+ identity of the isomeric state.

ACKNOWLEDGEMENTS

I would like to thank my supervisor, and research director, Dr. R. G. Summers-Gill, and past and present members of his research group. Their patience and assistance were greatly appreciated.

I extend my gratitude to the members of the Tandem Accelerator Laboratory, faculty, students, and staff with whom I have had many useful discussions, some of which were even related to my research topic, and whose friendships I value highly.

I would also like to express my thanks to Mrs. Helen Kennelly for her expertise in turning chicken scratchings, and thoughts into a typed manuscript.

Special thanks go to Arif Khan, and Albert Lee for their assistance with the experiments, and their advice which helped me "crank" out the results.

Finally, I would like to thank my wife, Carol. She not only had to put up with me during the writing of this thesis, but she also helped during some of the experiments, acted as my proof reader, messenger, drafts person (and did an excellent job, that is once I convinced her to use pen, and ink, as crayons were not acceptable), and was a constant source of inspiration. (I didn't plan this to sound like a Geritol commercial, it just happened!) I think I'll keep her.

This work is dedicated to my Mother, Father, sister
Andrea, and my wife, Carol.

(P.S. The paperback version of this thesis will soon be
published by Ripley's Believe It Or Not publishing company,
and will have a foreward written by (you guessed it)
the one, the only Hermit Pauli Nomial).

TABLE OF CONTENTS

		<u>Page</u>
CHAPTER 1	INTRODUCTION	1
CHAPTER 2	CONVERSION ELECTRON MEASUREMENTS	6
	(2.1) The Internal Conversion Process	6
	(2.2) Experimental Techniques	8
	(i) Target Preparation	8
	(ii) The Orange Spectrometer	8
	(iii) Pulsed Beam Conversion Electron Measurements	11
	(a) The Beam Pulsing System	11
	(b) The Electronics	13
	(c) Methods of Analysis	19
	(iv) In-beam Conversion Electron Measurements	25
CHAPTER 3	GAMMA RAY MEASUREMENTS	31
	(3.1) Energy Measurement and Efficiency Calibration	31
	(3.2) Excitation Function	32
	(3.3) Pulsed Beam Gamma Ray Measurements	35
	(3.4) In-beam Gamma Ray Measurements	37
CHAPTER 4	EXPERIMENTAL RESULTS AND DISCUSSION	42
	(4.1) Gamma Ray Measurements	42
	(4.2) Conversion Coefficient Measurements	44

	<u>Page</u>
(4.3) Development of the Decay Scheme for $^{146}\text{Eu}_m$	44
(4.4) The Recent Investigation by Ercan et al.	57
(4.5) Conclusions	58
REFERENCES	60

LIST OF TABLES

		<u>Page</u>
4.1	Results of the In-Beam Conversion Coefficient Measurements	45
4.2	Results of the Pulsed Beam Conversion Coefficient Measurements	46
4.3	Multipolarity Assignments and Total Transition Intensities	47
4.4	Estimate of the centroid energies of the $\pi(2d_{5/2})^{-1}\nu(2f_{7/2})$, $\pi(1g_{7/2})^{-1}\nu(2f_{7/2})^1$ and $\pi(\cancel{1h_{11/2}})^1\nu(2f_{7/2})^1$ multiplets.	49
4.5	Calculated and Observed Spectra for the $\pi(2d_{5/2})^{-1}\nu(2f_{7/2})^1$ Configuration of ^{146}Eu .	56

LIST OF FIGURES

		<u>Page</u>
1.1	The decay scheme for $^{146}\text{Eu}^m$ proposed by Hagemann et al. (1971), and Gavriilyuk et al. (1973).	4
2.1	The "Orange" beta ray spectrometer.	9
2.2	The McMaster University Tandem Accelerator and the "Orange" beam line.	12
2.3	The electronic circuit used for the pulsed beam conversion electron measurements.	14
2.4	A typical electron pulse height spectrum.	17
2.5	A typical "gated" electron pulse height spectrum.	18
2.6	Pulsed beam conversion electron spectrum for 33 Mev Li ions and a ^{142}Nd target.	
	(a) The spectrum from 1650-2000 Bp.	20
	(b) The spectrum from 2000-2450 Bp.	21
2.7	A typical time spectrum.	23
2.8	The decay curves of the $^{146}\text{Eu}^m$ conversion electron transitions.	24
2.9	The electronic circuit used for the in-beam conversion electron measurements.	28
2.10	In-beam conversion electron spectrum for 33 Mev Li ions and a ^{142}Nd target.	
	(a) The spectrum from 1500-1975 Bp.	29
	(b) The spectrum from 1975-2000 Bp.	30

	<u>Page</u>	
3.1	Excitation functions for selected gamma rays.	34
3.2	The electronic circuit used for the pulsed beam gamma ray measurements.	36
3.3	Pulsed beam gamma ray spectrum with $^{152,154}\text{Eu}$ calibrating source for 33 Mev Li ions and a ^{142}Nd target.	38
3.4	Pulsed beam gamma ray spectrum for 32.5 Mev Li ions and a ^{142}Nd target.	39
3.5	The electronic circuit used for the in-beam gamma ray measurements.	40
3.6	In-beam gamma ray spectrum for 33 Mev Li ions and a ^{142}Nd target.	41
4.1	Variation of the ratio of the in-beam intensities of the 358.2 and 377.0 keV gamma rays with beam energy.	43
4.2	The proposed decay scheme of the 0.230 ms isomer in ^{146}Eu .	50
4.3	A decay scheme for $^{146}\text{Eu}^m$ using an alternate placement of the 14.4 keV transition.	53
4.4	The decay scheme for $^{146}\text{Eu}^m$ proposed by Ercan et al. (1980).	59

CHAPTER 1

INTRODUCTION

The ^{146}Eu nucleus is an odd-odd nucleus which has one neutron outside the $N=82$ major shell, and one proton hole in the $Z=64$ shell. The single particle model might therefore be expected to be suitable to describe the odd-odd nucleus. Assuming this to be true, the ^{146}Eu nucleus is of interest since empirical values for the matrix elements of the neutron-proton two-body interaction could be extracted from its energy spectrum. The empirical values could then be used in shell model calculations in neighbouring nuclei.

The ground state spin of ^{146}Eu has been measured as $\frac{1}{2}^-$ by Ekström et al. (1972) in an atomic beam experiment. Early investigators studied the excited states of ^{146}Eu by observing the electron capture decay of the 0^+ ground state of ^{146}Gd which populates low spin states of ^{146}Eu . Since the ^{146}Gd decay is first forbidden ($\log ft = 8.5$) and the subsequent gamma ray transitions leading to the ground state of ^{146}Eu were found by these investigators to have M1 multipolarities, the ground state of ^{146}Eu was therefore assigned negative parity. Remayev et al. (1962) using the $(p,2n)$

reaction on ^{147}Sm reported the existence, in ^{146}Eu , of an isomer with a half-life of $240 \pm 10 \mu\text{s}$. Although delayed gamma ray transitions of 240, 280, 360, 390 and 480 keV were reported, no decay scheme was established. An investigation by Rakevnenko et al. (1968) determined the energy of one gamma ray transition in the decay to be 276 keV. They also found it to have an E2 or M1 nature, by virtue of its K/L conversion electron ratio. Subsequent investigations by Hagemann et al. (1971), and Gavriilyuk et al. (1973), using the $(^{12}\text{C}, 5n)$ reaction on ^{139}La , resulted in the formulation of the decay scheme shown in Figure 1.1. These investigators were able to measure the energies, and relative intensities of four gamma ray transitions which they identified as being involved in the isomeric decay. The tentative assignment of spins and parities to the energy levels shown in Figure 1.1 resulted from shell model considerations. On the basis of the shell model, a 9^+ isomer was an attractive idea. The isomeric transition, however, could not be identified.

The relative weakness of Eu K x-rays in the ^{146}Eu spectrum has led to the belief that the unseen isomeric transition must have an energy which is less than 48.5 keV (the K shell binding energy of Eu). Such a low energy 9^+ to 6^- transition would have a longer half-life than that measured for $^{146}\text{Eu}^m$. The unseen isomeric transition is therefore expected to occur between the 9^+ and 7^- states, and be highly

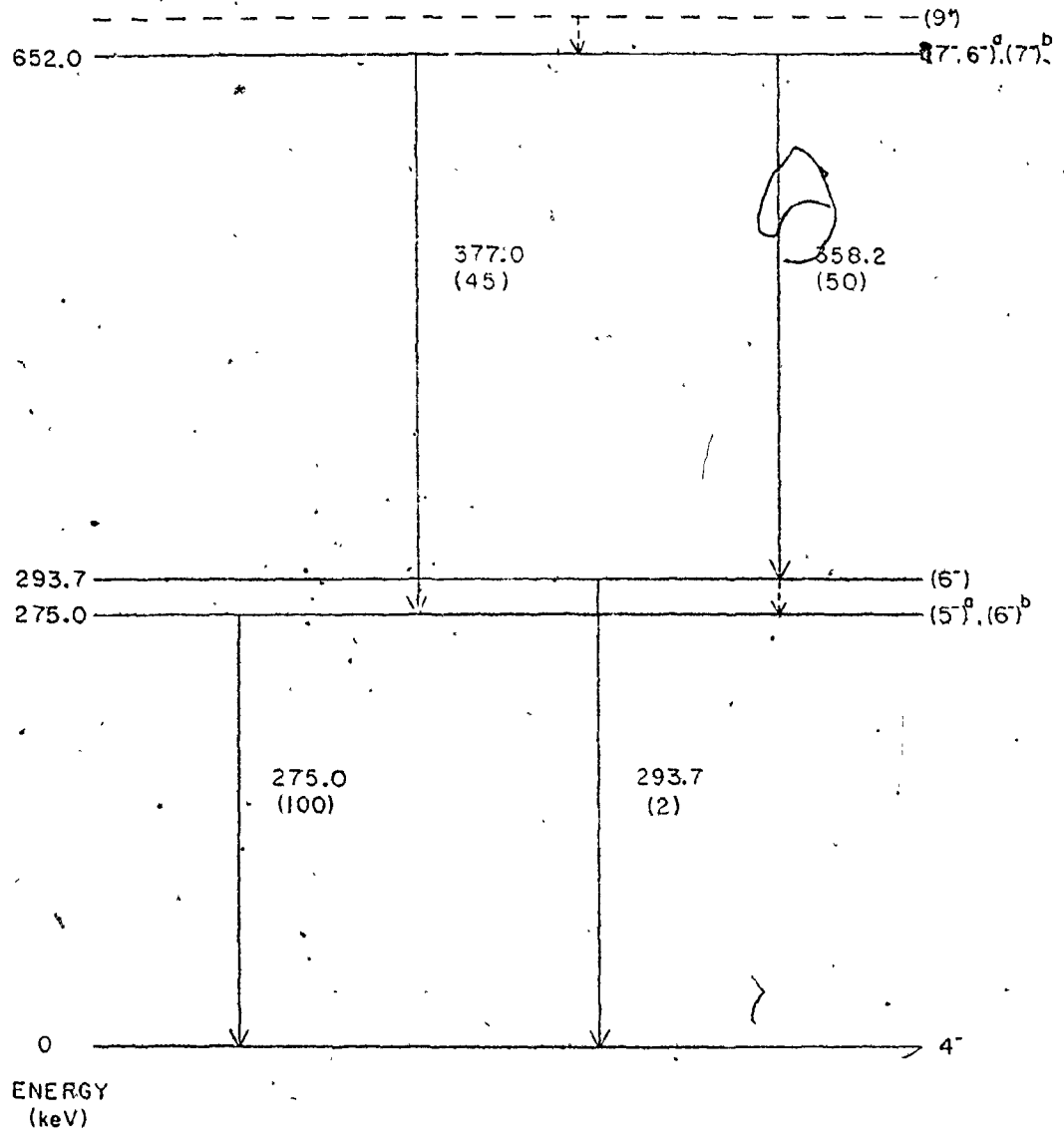
converted. However, it would not be possible to get from the 7^- excited state to the 4^- ground state of ^{146}Eu by a cascade of only two M1 gamma rays, and in this mass range low energy E2-transitions are not very likely to occur if competing M1 transitions are possible. This difficulty would be removed if one more transition were involved in the cascade, contrary to the decay scheme shown in Figure 1.1. Further doubt has been cast on this decay scheme by gamma ray studies carried out at McMaster University by Summers-Gill and Wender (1975) using the $(p,2n)$ reaction on ^{147}Sm , the $(^7\text{Li},3n)$ reaction on ^{142}Nd , and a beam of 45 Mev ^{10}B on natural Ce. They determined that the intensities of the 358.2 and 377.0 keV transitions were inconsistent with their placement in Figure 1.1. Using a Si(Li) detector they were also able to detect a delayed 14.4 keV transition not previously reported. However, Summers-Gill and Islam (1973) established that the 358.2 and 377.0 keV gamma rays were both in coincidence with the 275.0 keV gamma ray, but not in coincidence with each other. This is consistent with the placement of these lines in the decay scheme shown in Figure 1.1.

Although shell model considerations, and the McMaster investigations cast severe doubts on the proposed $^{146}\text{Eu}^m$ decay scheme, they were not sufficient to firmly establish an alternate decay scheme as the multipolarities of the decay transitions were not known. The present investigation was

Figure 1.1

The decay scheme for $^{146}\text{Eu}^m$ proposed by Hagemann et al. (1971), and Gavriilyuk et al. (1973).

$T_{1/2} = 235 \mu s$



therefore initiated to determine the multipolarities of the transitions associated with the decay of $^{146}\text{Eu}^m$. It was hoped that with this knowledge the decay scheme would be clarified.

Subsequent to the present investigation, but prior to the writing of this thesis, Erçan et al. (1980) published the results of their investigation of the isomer. Their results will be discussed in a later chapter.

CHAPTER 2

CONVERSION ELECTRON MEASUREMENTS.

(2.1) The Internal Conversion Process

A transition between nuclear states results in a change in the nuclear multipole field. If this change is mediated by an electromagnetic coupling of the nucleons, and the surrounding electromagnetic field, then a gamma ray will be emitted to carry away the excess energy and angular momentum. However, if the change is mediated by a coupling of the nucleons, the surrounding electromagnetic field, and an orbiting atomic electron, then the excess energy and angular momentum can be transferred to the electron. This process is called internal conversion. It is the nuclear analogy of the Auger effect in atomic physics. The energy given to the electron is obviously:

$$E_E = E_\gamma - E_{B.E.} \quad (2.1)$$

where $E_{B.E.}$ is the binding energy of the electron, and E_γ is the energy released in the nuclear transition. Several discrete electron lines appear for each value of E_γ , corresponding to electrons being ejected from the different atomic shells, ie K, L_1 , L_{11} , L_{111} , etc.

Internal conversion and photon emission are independent, competing decay processes. The ratio of the rate of

electron emission to the rate of photon emission is defined as the internal conversion coefficient, α . The conversion coefficient is essentially independent of nuclear structure. It depends strongly on the energy of the nuclear transition, the electronic wavefunction (which is defined by the charge number, Z), and the multipolarity of the transition. Since the electronic wavefunctions are well known, precise tables of theoretical conversion coefficients have been constructed for each Z , as a function of energy, multipolarity, and the orbital shell of the expelled electron. A measurement of the K shell conversion coefficient, α_K , can therefore be an effective means of determining the multipolarity of a nuclear transition. As well, the multipolarity can sometimes be determined from the ratio of the number of electrons in the K shell peak to the number of electrons in the L shell peaks associated with a particular transition, that is α_K/α_L . A much more sensitive measure, though, is the ratio of the number of electrons in the L_1 , L_{11} and L_{111} peaks. High resolution is required for such a comparison. In practice, a measurement is usually made of the K shell conversion coefficient, and the α_K/α_L ratio of conversion electrons.

(2.2) Experimental Techniques

(i) Target preparation

The levels in $^{146}\text{Eu}^m$ were populated by the ($^7\text{Li}, 3n$) reaction on ^{142}Nd using a 33 Mev beam of ^7Li ions. The energy was chosen on the basis of gamma ray excitation function measurements that will be discussed in the next chapter. Neodymium was obtained from Oak Ridge National Laboratory in the form of Nd_2O_3 enriched to greater than 98% Neodymium-142. The Nd_2O_3 was reduced by heating in vacuum with ThO_2 to form a metal pellet which was then rolled to produce a target of 8.0 mg cm^{-2} thickness. The same target was used in all conversion electron, and gamma ray experiments. It was kept under vacuum between experiments to prevent oxidation.

(ii) The Orange spectrometer

The pulsed, and in-beam conversion electron spectra were obtained using a seven-gap orange spectrometer. To measure the magnetic field, a Rawson probe occupies one of the seven gaps. Electrons emitted from the target are focussed by the remaining six gaps on to a plastic detector, 1 cm. in diameter (see Figure 2.1).

The circular path of a charged particle moving in a magnetic field is described by the equation

$$B\rho = p/q$$

where p = momentum of the particle

q = charge of the particle

B = component of the magnetic field perpen-

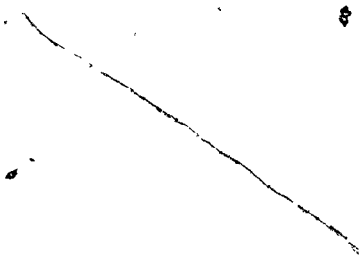
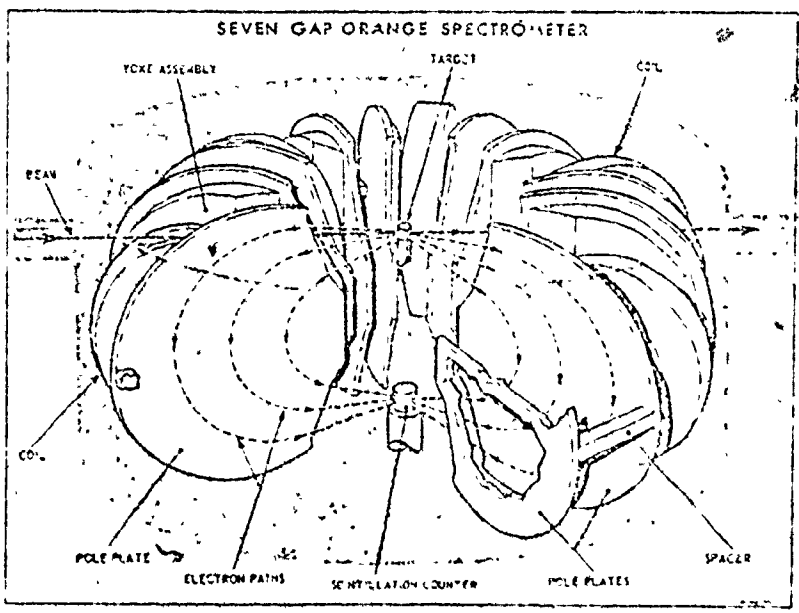
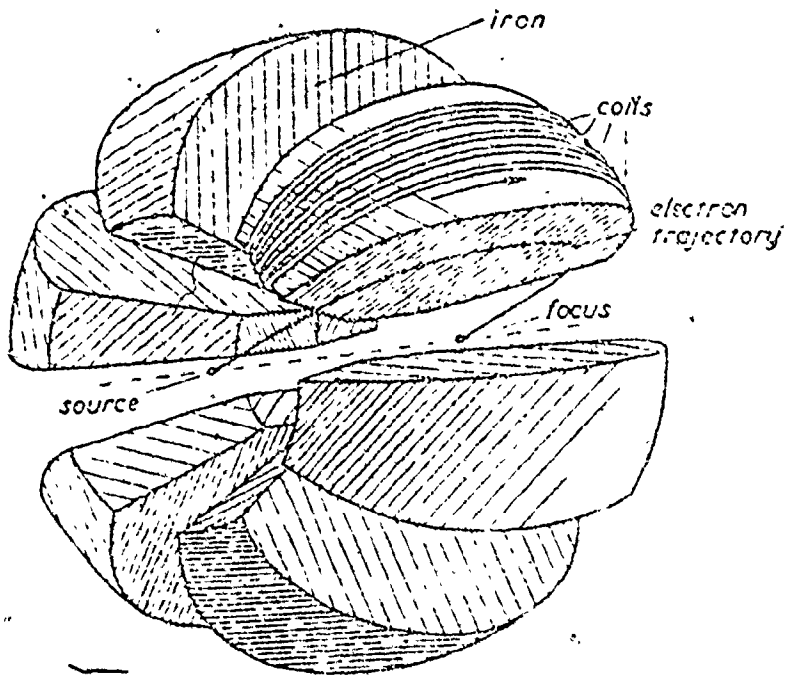


Figure 2.1

The "Orange" beta-ray spectrometer (from Geiger (1965)).



dicular to the path

ρ = radius of curvature.

($B\rho$ is called the magnetic rigidity of the particle.)

In the orange spectrometer, ρ , the radius of curvature, is fixed. Particles of different momenta can therefore be focussed on to the detector by changing the magnetic field, B . A spectrum of conversion electrons can be obtained by systematically varying the magnetic field, and counting the number of electrons detected for a fixed number of nuclear reactions. A good measure of the number of nuclear reactions is given by the number of ${}^7\text{Li}$ ions which are elastically scattered at some fixed angle to the beam. A second plastic scintillator located 52° to the beam axis facilitates this measurement.

The integrated beam current, as collected in a Faraday cup beyond the spectrometer, is also recorded at each setting of the magnetic field. The ratio of the integrated beam current to the number of elastically scattered lithium ions is a good indicator of the condition of the target. The time taken to record the preset number of elastically scattered ${}^7\text{Li}$ particles is also recorded. If the beam was off for any appreciable time during one setting there would be a larger than normal background contribution to the electron count for that setting. However, if this were to happen, the counting time would be longer than normal. The counting time can therefore be helpful in pinpointing such unreliable data points.

The spectrometer was set up to automatically print out on a teletype, the number of elastically scattered ${}^7\text{Li}$ particles, the number of electrons, the counting time, the integrated beam current, and the momentum ($B\rho$), at each setting. Once these had been recorded the scalers were zeroed, the magnetic field stepped by a preset amount, and counting was resumed.

Further information on the orange spectrometer has been given by Khoo (1972).

(iii) Pulsed beam conversion electron measurements

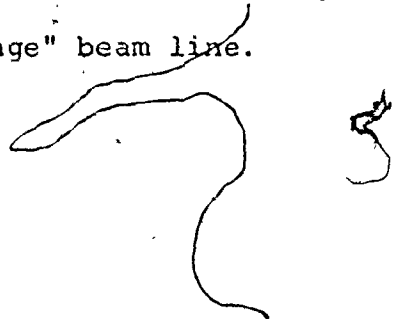
(a) The Beam Pulsing System

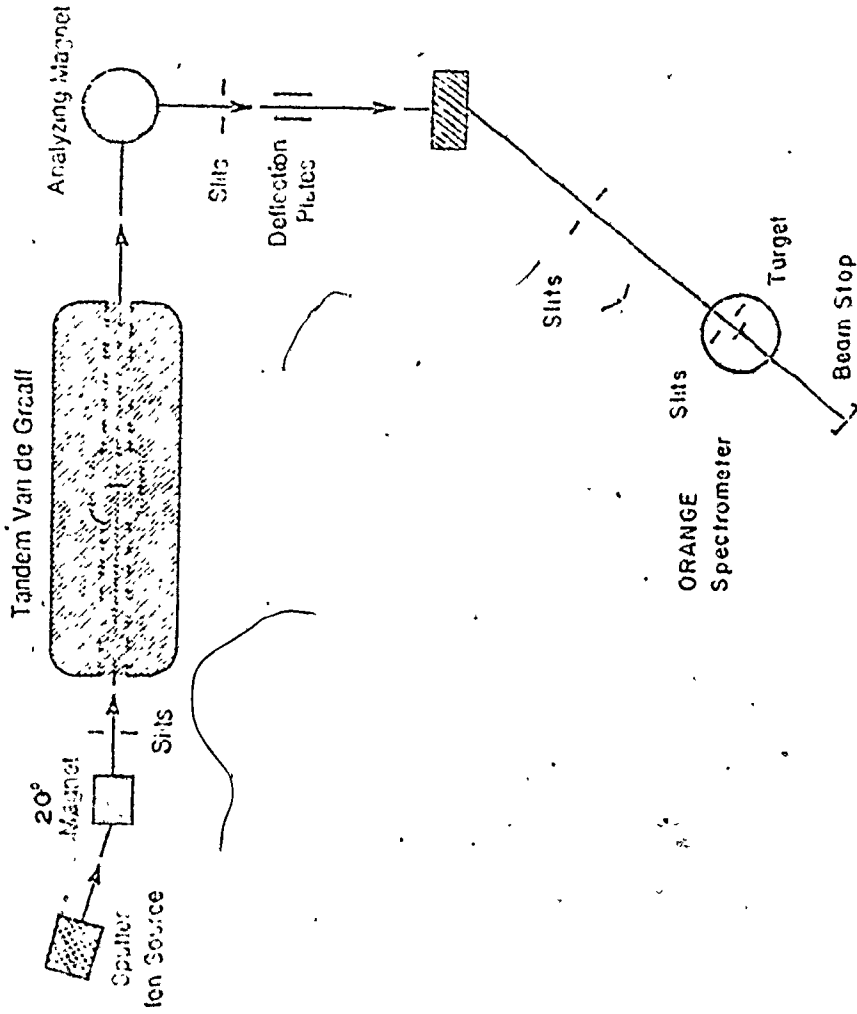
A pulsed beam experiment, with the conversion electrons being measured during the beam-off periods, was performed to eliminate the conversion electrons coming from prompt transitions, thereby simplifying the analysis, improving the signal to noise ratio, and allowing the K peak from the very weak 293.9 keV line to be detected.

Figure 2.2 is a schematic drawing of the McMaster University Tandem Accelerator, and the "Orange" beam line. The beam was pulsed at the deflection plates which were charged to +2000 volts. Pulsing was achieved by sending a square wave signal from a pulser to a driving circuit connected to the plates. When the signal was positive, the right hand plate became essentially shorted to ground, and the beam was deflected by approximately 0.5° . When the signal was null, both plates

Figure 2.2

The McMaster University Tandem Accelerator, and the
"Orange" beam line.





were again charged to +2000 volts, and the beam was allowed to pass undeflected. A set of slits was installed at a waist in the beam, after the switching magnet and the next set of quadrupole magnets on the "Orange" beam line, to prevent the deflected beam from reaching the target area and producing unwanted background counts. The beam-off time was arranged to be 0.5 ms, with a beam-on time of 0.5 ms. The response time of the driving circuit was very short compared to the beam-on and beam-off time periods. Likewise, the beam transit time from the deflecting plates to the target area is negligible on this time scale.

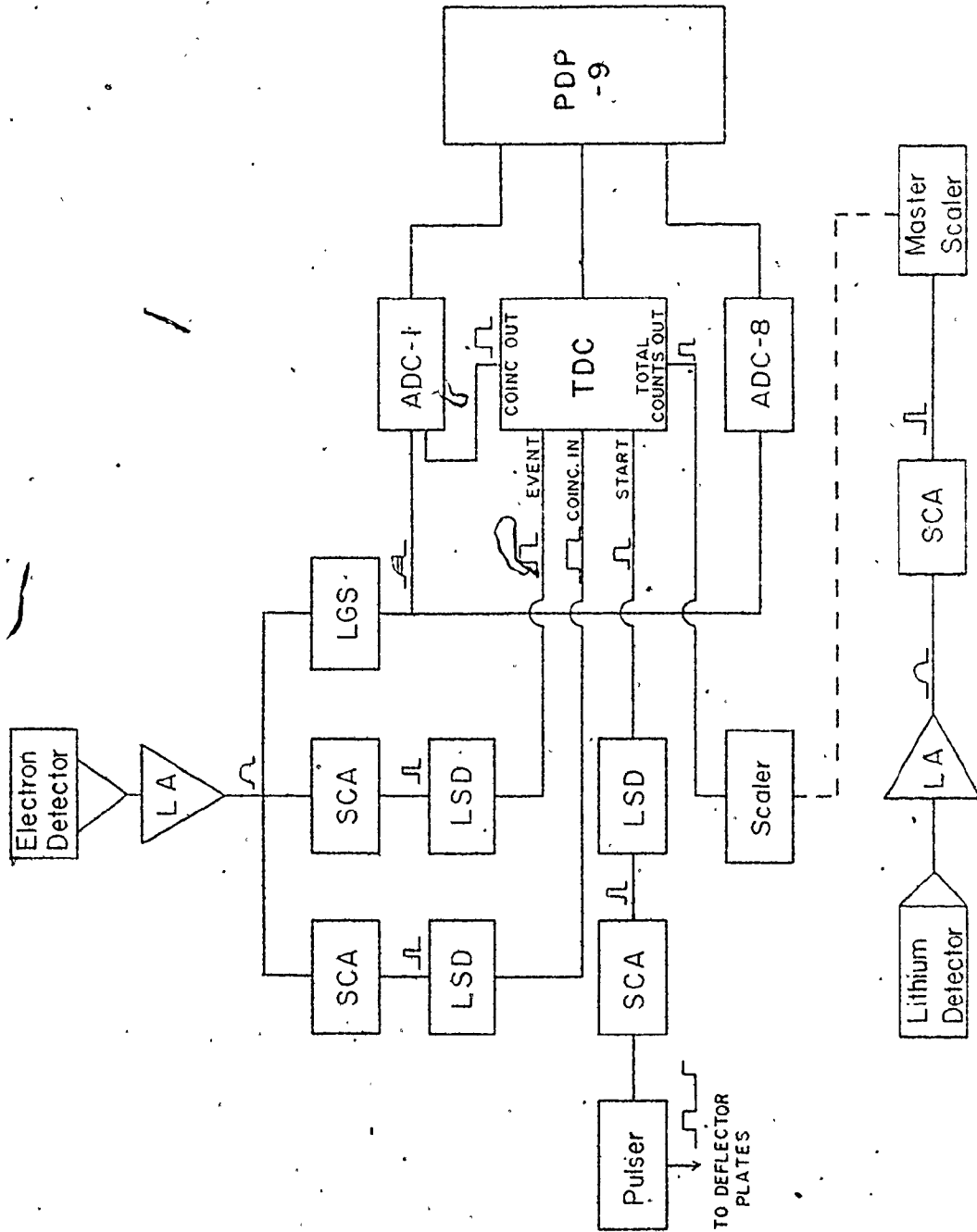
(b) The Electronics

The electronics used in the pulsed beam conversion electron experiment are shown schematically in Figure 2.3. The "heart" of this circuit is the Time to Digital Converter (TDC) which was specially designed by R. A. McNaught for this type of an experiment. The TDC is designed to measure time intervals (the time between a start signal and an event signal) that are longer than can be measured with a commercially available Time to Amplitude Converter (TAC). The clock rate of the TDC is selected by a panel switch (CHANNEL WIDTH) and is generated by counting down the pulses from a 20 MHz crystal-controlled oscillator. Another important feature of the TDC is that it will record the times of arrival of more than one event for each start signal. This permits data to be accumu-

Figure 2.3

The electronic circuit used for the pulsed beam conversion electron measurements. The symbols used are explained below.

Abbreviation	Explanation
LA	linear amplifier (ORTEC 452, TC203BLR)
LGS	linear gate and stretcher (ORTEC 442)
SCA	single channel analyser (CANBERRA 1436)
OR	universal coincidence (ORTEC 418A) set to give an output for one "coincident" pulse
LSD	logic shaper and delay (CI 1455)
D	delay amplifier (ORTEC 427)
TDC	time-to-digital converter
PDP-9	Digital Equipment Corporation computer
PULSER	pulse generator (DATA PULSE 101)



lated at a higher rate than with a conventional single stop TAC. The TDC also allows for an adjustable delay of from 0 to 10 μs to be inserted between the time of arrival of the start signal, and the time when event signals will be accepted by the TDC. This can be used to correct for the finite time of flight of the bombarding particles, and thereby insure that counts are only accepted during beam-off periods. As well, a set of back-off switches, which represent digitally accurate delays, may be used to shift the time period during which event signals are to be accepted.

The TDC was connected to the PDP-9 computer as an ADC, and was used in the coincidence mode. In this mode, the TDC stores the time of arrival of the event signal, and remains busy until all of the associated coincident ADC's have completed their conversions, when all are read by the computer. Another event may then be accepted if the chosen time period has not yet elapsed. The TDC has a region length of 1 K, and a channel width of 0.4 μs was selected, thus giving a total live time of 400 μs . It should be noted that the TDC can also be used in the singles mode. In this mode it operates as an ADC does in the singles mode.

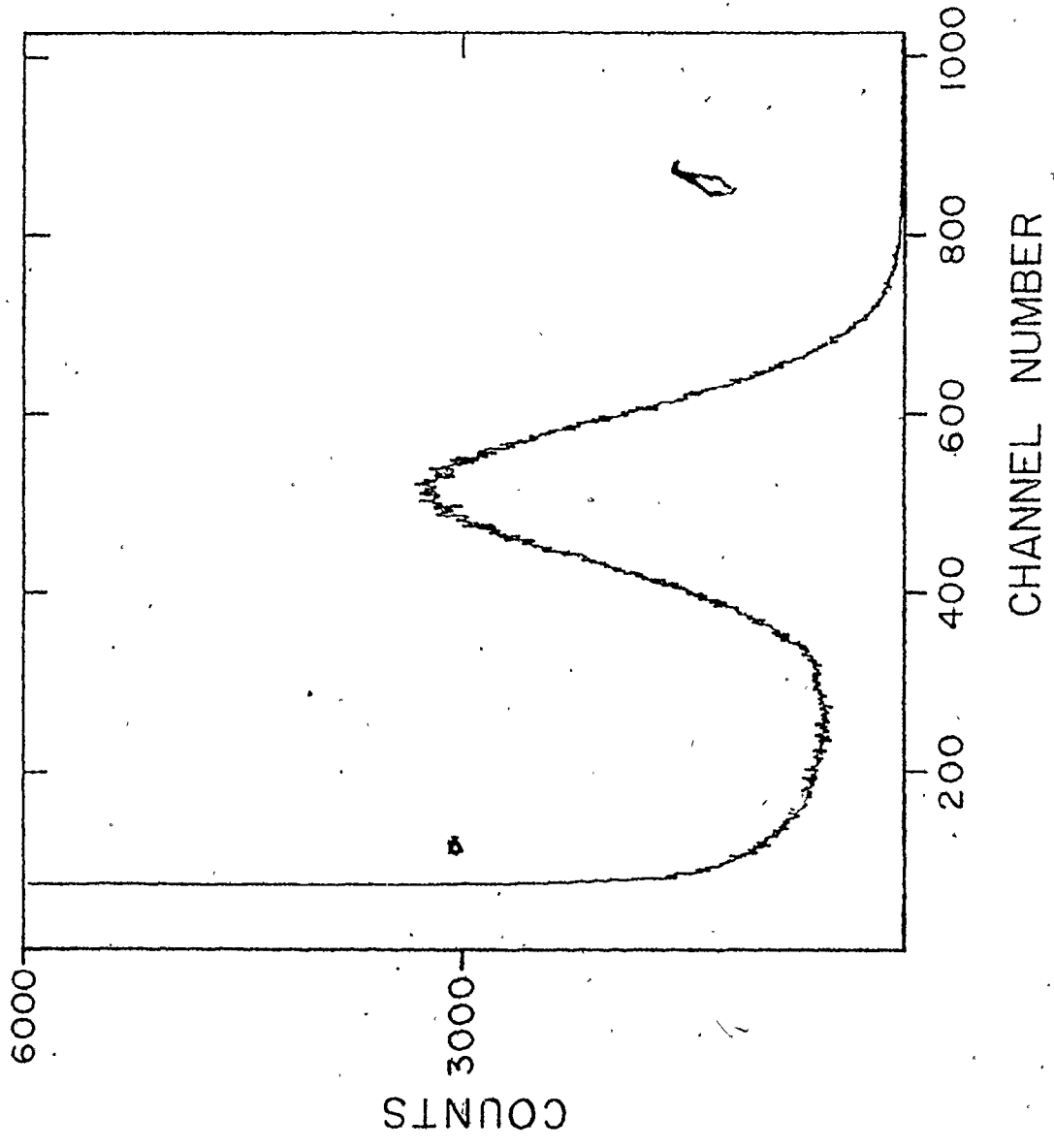
The signal from the pulse generator that initiates the deflection of the beam, also served as the start pulse for the TDC. This ensures that the TDC will only accept counts which arrive during beam-off time periods.

Both an event and a coincidence signal were fed into the TDC which required a coincidence between these two signals before a count would be accepted. The coincidence out signal, which will only be high when an event signal has been accepted by the TDC, was used as the gating signal for the associated coincidence ADC's. The TDC can also be operated in the anti-coincidence mode.

The signal entering the COINCIDENCE IN of the TDC was used as a pulse height gating signal. A typical pulse height spectrum obtained with the plastic scintillation detector of the orange spectrometer at a B_0 value of 1752 gauss-cm is shown in Figure 2.4. One can distinguish the monoenergetic electron peak, the relatively flat background below this peak, which is caused by electrons backscattered from the detector, and a sharply rising low energy tail. The low energy tail, which results from electronic noise, and γ -rays, can only be rejected at the expense of losing some of the backscattered electrons. A typical spectrum employing the pulse height gating signal is shown in Figure 2.5. This spectrum was collected at the same time as the spectrum shown in Figure 2.4. The fraction of the electron events not accepted by virtue of the fixed threshold level is obviously a function of the transition energy, and therefore, a correction must be made. To this end, the electron pulse height spectrum (Figure 2.4), and the gated pulse height spectrum (Figure 2.5) were recorded for each peak in the conversion electron spectrum.

Figure 2.4

A typical electron pulse height spectrum. The detector was a plastic scintillator, and the "Orange" beta ray spectrometer was set at B_0 value of 1752 gauss-cm.



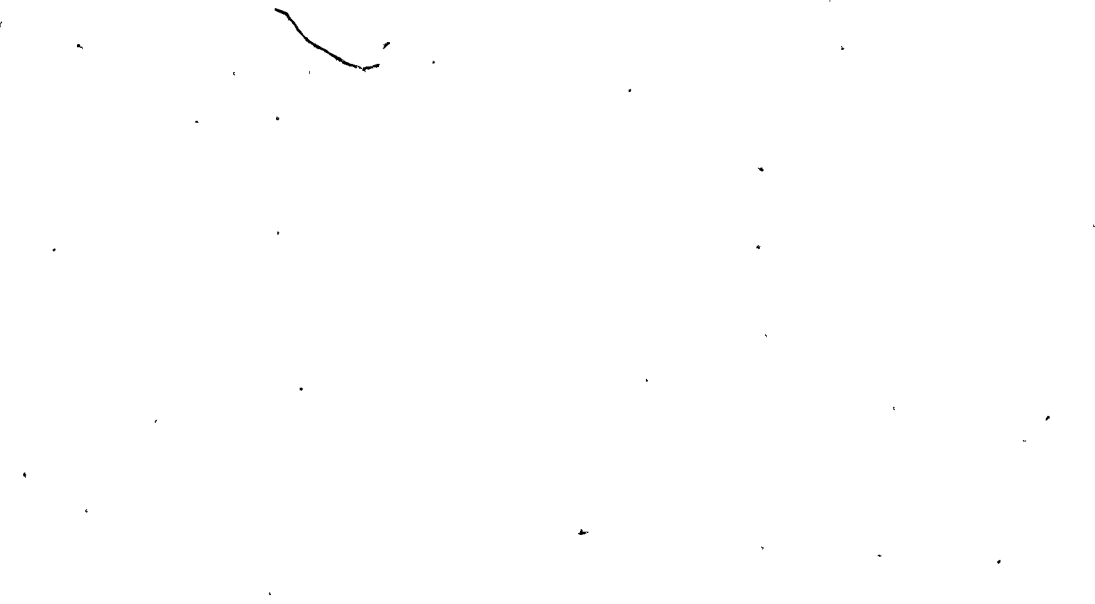
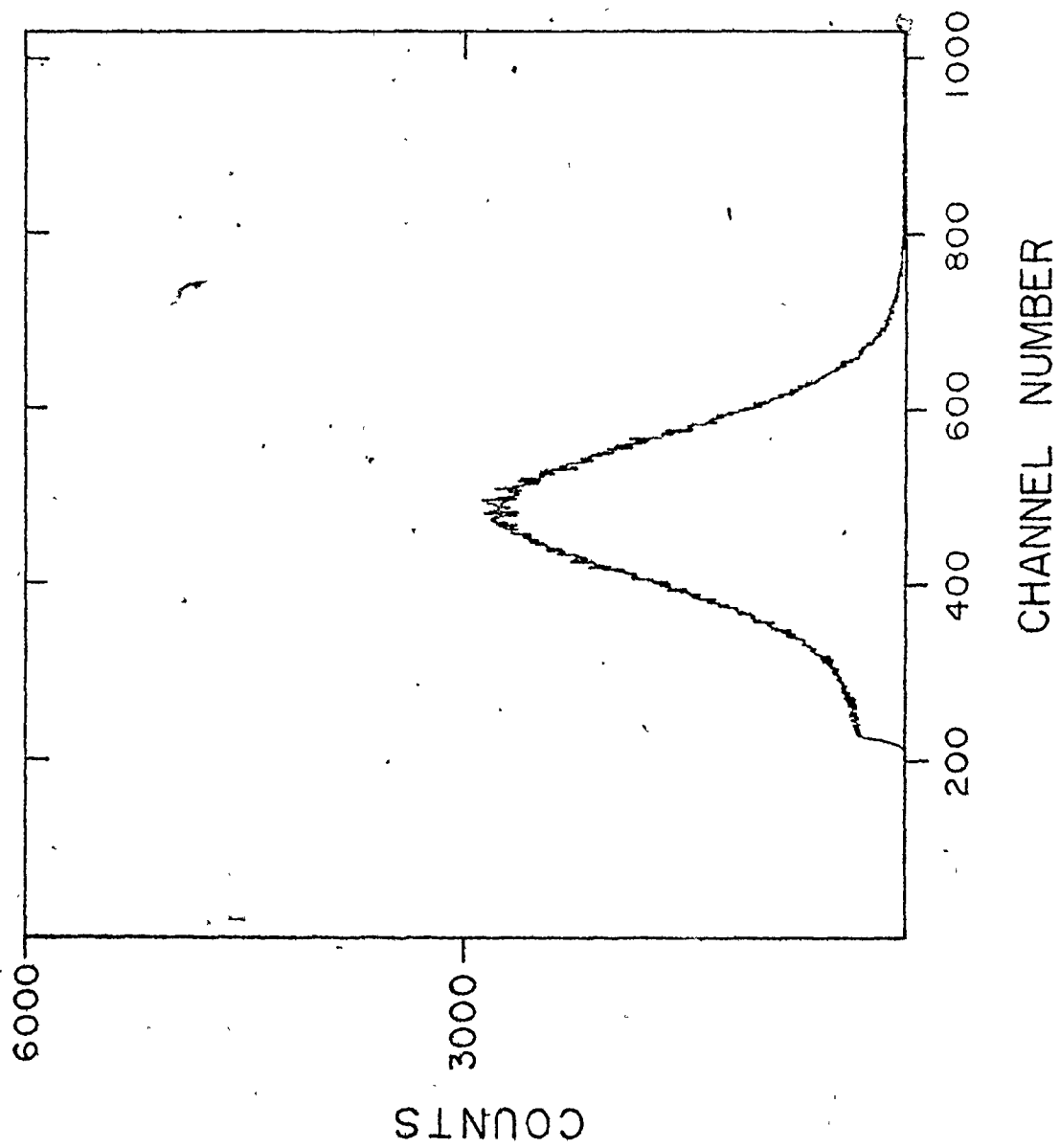


Figure 2.5

A typical "gated" electron pulse height spectrum. These data were collected at the same time as the electron pulse height data shown in Figure 2.4.



The signal taken from the TOTAL COUNTS OUT of the TDC was fed to a scaler to accumulate the number of electrons detected at each setting of the magnetic field.

(c) Methods of Analysis

The pulsed beam conversion electron spectrum is shown in Figure 2.6. It has been analysed with the use of the CDC 6400 computer, and the program ANABEL. This program was written and a detailed account of the program was given, by Henryk Mach. It is based on the program JAGSPOT written originally at Chalk River, and developed by various members of the McMaster β - and γ -ray spectroscopy group. Briefly, ANABEL performs a least squares fitting routine to a peak shape which is the convolution of an exponential (decreasing towards lower energy) and a Gaussian. This can be expressed mathematically by:

$$I(x) = \alpha + \beta x + \sum_{j=1}^N \gamma_j \int_{-\infty}^{A_j} e^{\epsilon(y-A_j)} e^{-\delta(x-y)^2} dy$$

where x = channel number

$I(x)$ = counts in channel x .

N = number of peaks

$\alpha + \beta x$ = linear background term

γ_j = intensity of the Gaussian located at A_j

δ = width of the Gaussian

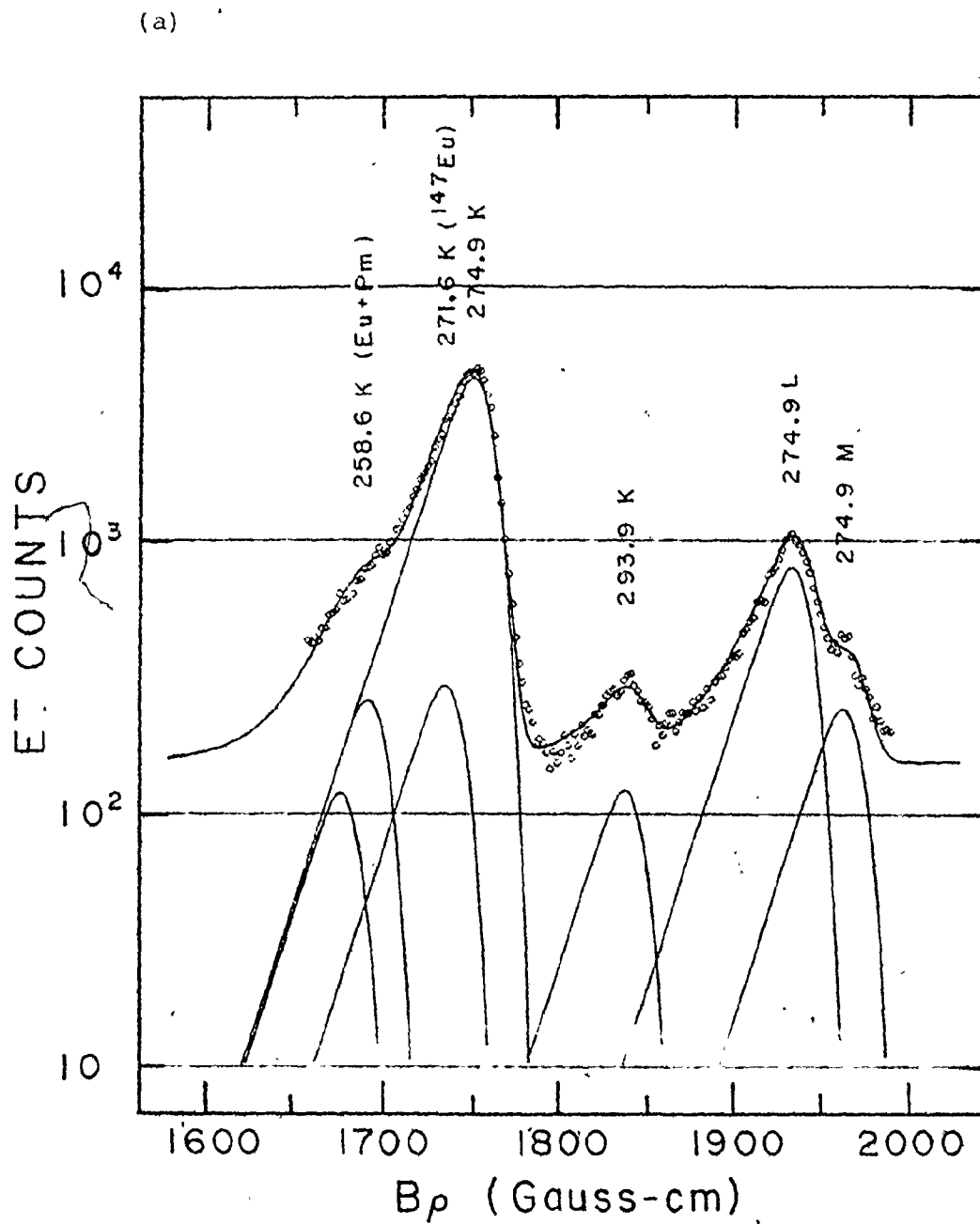
ϵ = constant determining the fall-off of the exponential tail

A_j = peak position of peak j .

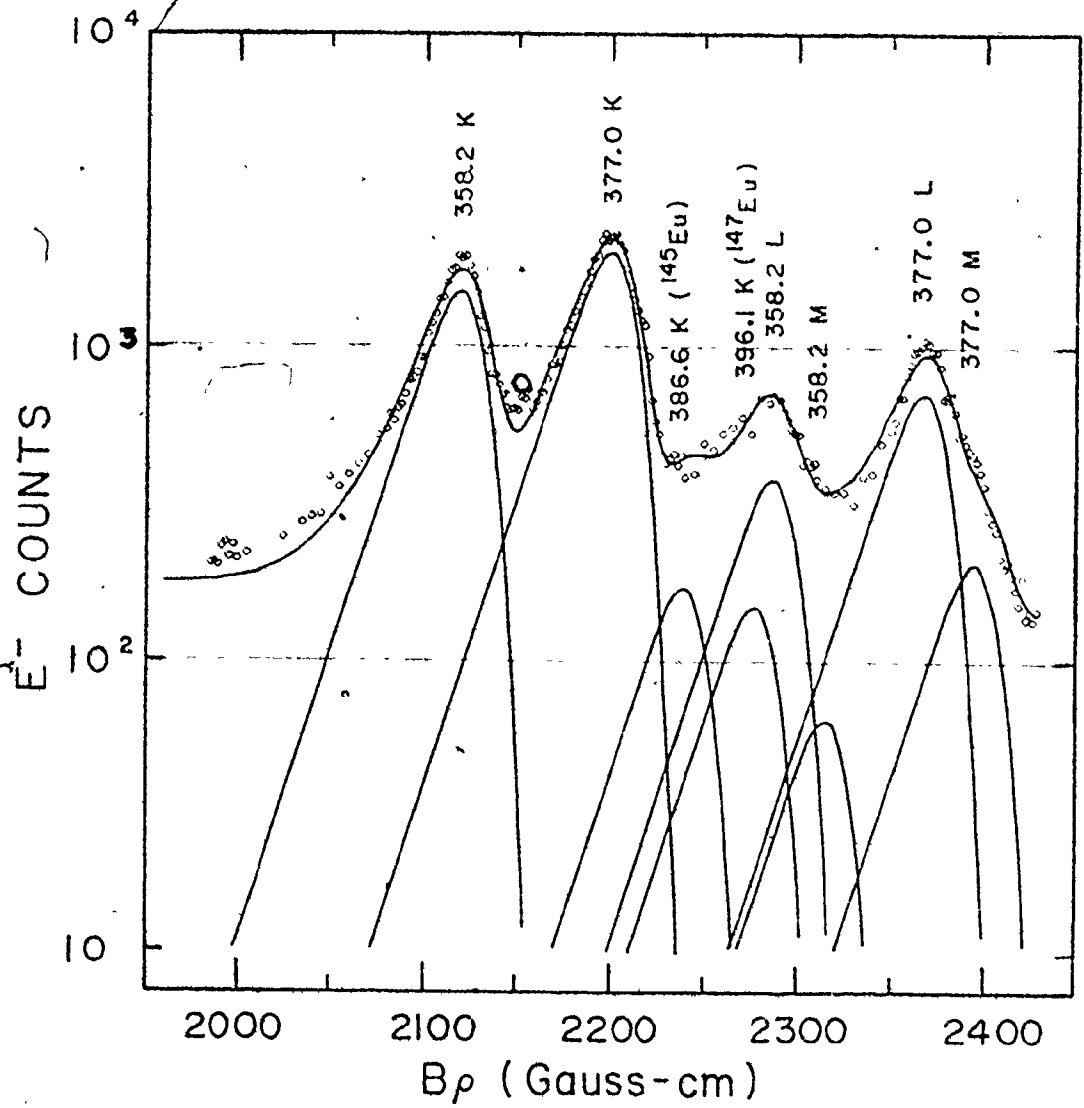
Figure 2.6

Pulsed beam conversion electron spectrum for 33 Mev Li ions and a ^{142}Nd target. Each point was collected for the time it took to accumulate 20,000 elastically scattered ^7Li ions in the particle detector. The average pulsed beam current was 5 nA.

- (a) The spectrum from 1650-2000 Bp.
- (b) The spectrum from 2000-2450 Bp.



(b)



In the program the relative positions of two or more peaks can be fixed. This allows one to fit K, L, and M shell peaks, whose separation is determined by the electron binding energies for a particular atomic number.

The half-life of the ^{146}Eu isomer was determined from the spectra collected by the TDC during the pulsed beam conversion electron experiment. The decay of each K-shell electron peak was determined from the TDC spectrum collected at the magnetic field setting of the maximum for that peak. A beam-off time of 1800 μs , with a beam-on time of 800 μs , was chosen for these measurements. The channel width of the TDC was selected to be 1.6 μs , thus giving a total rundown time of 1600 μs . The TDC spectrum taken at a setting of 1752 gauss-cm is shown in Figure 2.7. To improve the presentation, the points in the time spectrum were added together in groups of 50, and the results plotted on a semi-log graph. A weighted least squares fit to a decaying exponential with constant background was made, using a computer program written for the CDC 6400, to determine the half-life. The results are shown in Figure 2.8. No correction need be made to half-lives determined in this manner because of the accuracy of the timing system which was based on a crystal-controlled oscillator, and because the TDC accepts multiple events in one time period. In contrast, data collected by the use of a TAC (time to amplitude converter) must be corrected for the fact that, being a single stop unit, it will be preferentially stopped early

Figure 2.7

A typical time spectrum. The B_0 value was 1752 gauss-cm, with the channel width of the spectrum chosen to be 1.6 μ s.

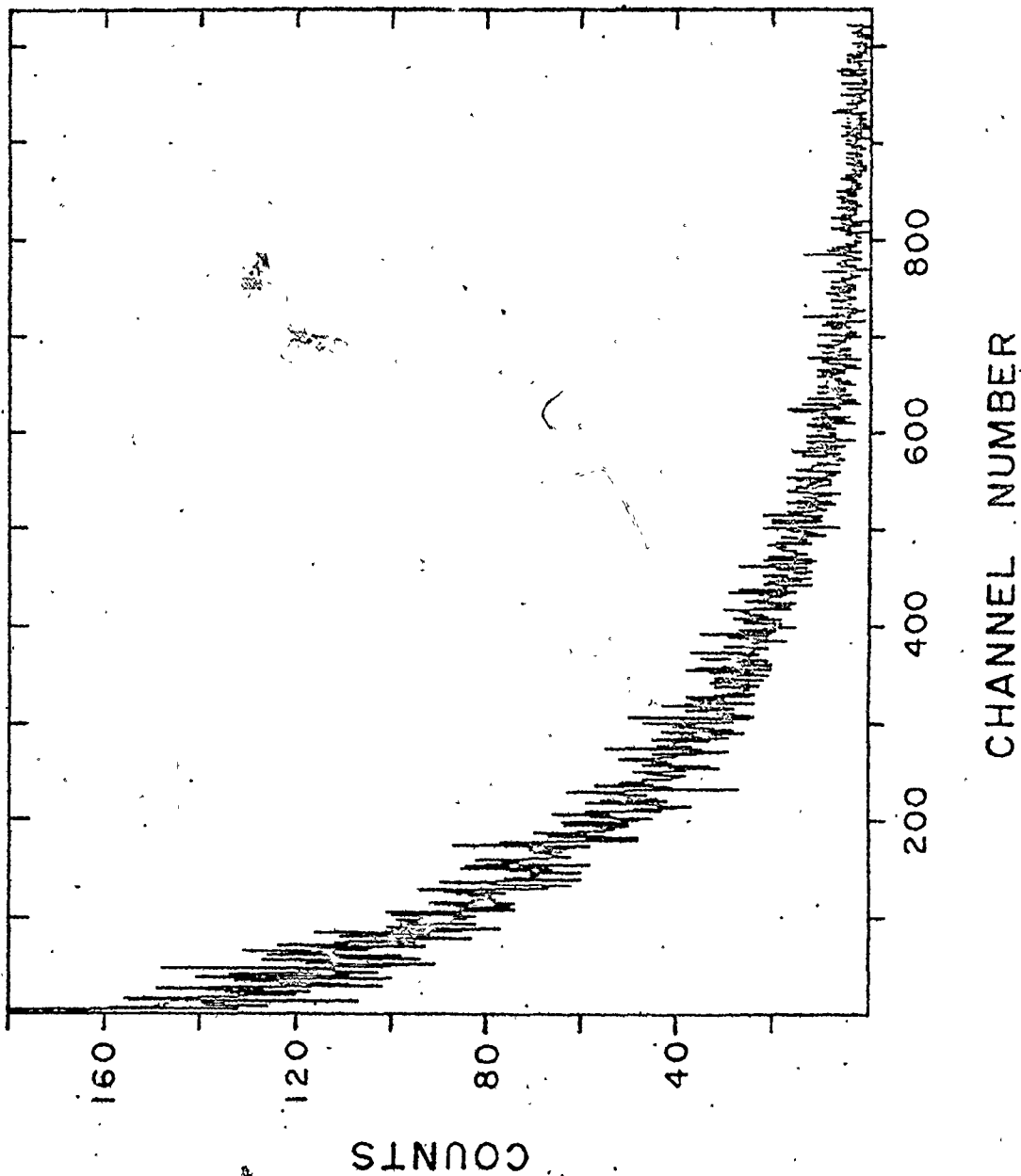
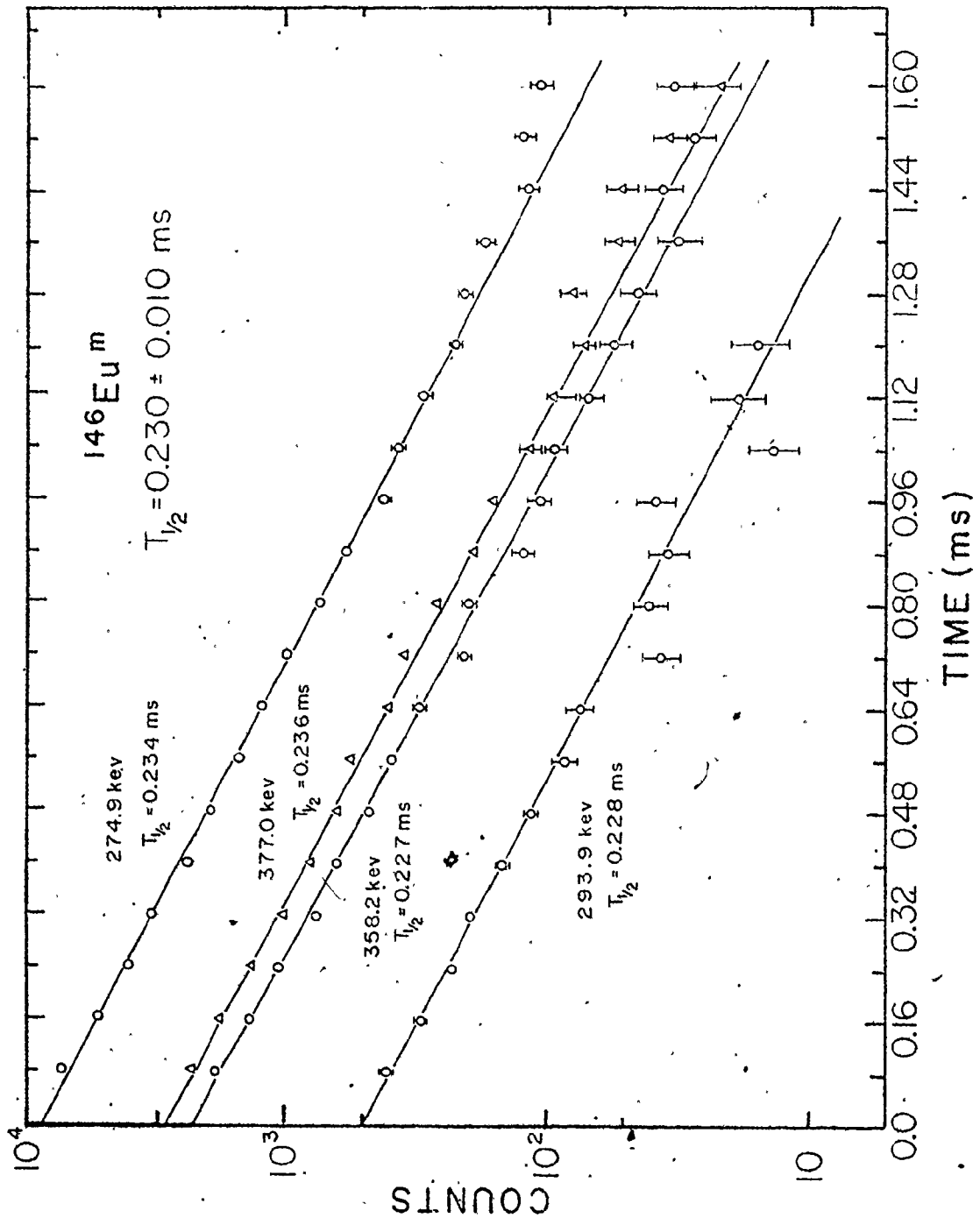


Figure 2.8

The decay curves of the $^{146}\text{Eu}^m$ conversion electron transitions.



in the measurement period yielding a value which is shorter than the true half-life.

(iv) In-beam Conversion Electron Measurements

The K shell conversion coefficient, α_K , is defined as the ratio of the rate of K shell electron emission to the rate of gamma ray emission. Empirically it can be calculated as

$$\alpha_K(E) = \frac{\frac{4\pi}{\Omega_e} \frac{1}{R_e} \frac{1}{B\rho} \frac{N_e}{\epsilon_e}}{\frac{4\pi}{\Omega_\gamma} \frac{1}{R_\gamma} \frac{N_\gamma}{\epsilon_\gamma}} = \frac{C \frac{1}{B\rho} \frac{N_e}{\epsilon_e}}{\frac{N_\gamma}{\epsilon_\gamma}} \quad (2.1)$$

- where
- E = energy released in the nuclear transition
 - Ω_e = solid angle subtended by the electron detection system at the target
 - Ω_γ = solid angle subtended by the gamma ray detector at the target
 - $R_\gamma; R_e$ = measures of the number of nuclear reactions which are used to normalize the electron and gamma ray data
 - ϵ_e = correction for the electrons lost due to the background suppressing discrimination level of the SCA
 - ϵ_γ = GeLi photo-peak efficiency
 - N_e = Number of counts in the K shell conversion peak

N_Y = number of counts in the gamma ray photo-peak
 C = essentially a constant over a small range of energy.

In principle, the solid angles subtended by the electron, and gamma ray detectors at the target could be determined, and the measurements could be suitably normalized. However transitions whose K shell conversion coefficients are known are normally used as calibrants. A calibrant can be used to determine the value of "C" in equation 2.1.

The pulsed beam conversion electron experiment was performed to eliminate the conversion electrons coming from prompt transitions. As a result, no suitable calibrants could be found in the pulsed beam conversion electron spectrum. An in-beam experiment was therefore also performed to determine the conversion coefficients of the 274.9 and 377.0 keV transition, the strongest transitions observed in the pulsed beam conversion electron spectrum of the decay of $^{146}\text{Eu}^m$, by using the 229.5 keV (M1+E2) and the 396.1 keV (M2) transitions in ^{147}Eu as calibrants. Having established the conversion coefficients of the 274.9 and 377.0 keV transitions, these lines could then be used as calibrants for the pulsed beam data. The excited states in ^{147}Eu are populated by the competing $^{142}\text{Nd}(^7\text{Li}, 2n)$ reaction, with the 229.5 and 396.1 keV transitions being the strongest observed transitions in ^{147}Eu . The K

shell conversion coefficients of the 229.5 and 396.1 keV transitions were taken to be those measured by Grigorev et al. (1977), i.e. $\alpha_K = 0.145 \pm 0.010$, and $\alpha_{K'} = 0.119 \pm 0.007$ respectively.

The electronics used for the in-beam conversion electron experiment are shown schematically in Figure 2.9. The output of the SCA was fed into a scaler to accumulate the electron counts. Once again, the pulse height (ADC1), and gated pulse height (ADC2) spectra were recorded for each peak to be used to correct for the loss of electron events resulting from the fixed threshold level of the SCA.

The in-beam conversion electron spectrum was fitted using the program ANABEL, and is shown in Figure 2.10. This spectrum is quite different than the pulsed beam conversion electron spectrum (Figure 2.6). There are fewer peaks in the pulsed spectrum, and the difference in the relative intensities of the 358.2 and the 377.0 keV K shell peaks is striking. The 293.9 keV K shell peak, which is clearly visible in the pulsed beam spectrum, is not apparent in the in-beam spectrum.

The discussion will now centre on the gamma ray measurements without which the K shell conversion coefficients, α_K , could not be determined.

Figure 2.9

The electronic circuit used for the in-beam conversion electron measurements. The symbols are the same as those used in Figure 2.3.

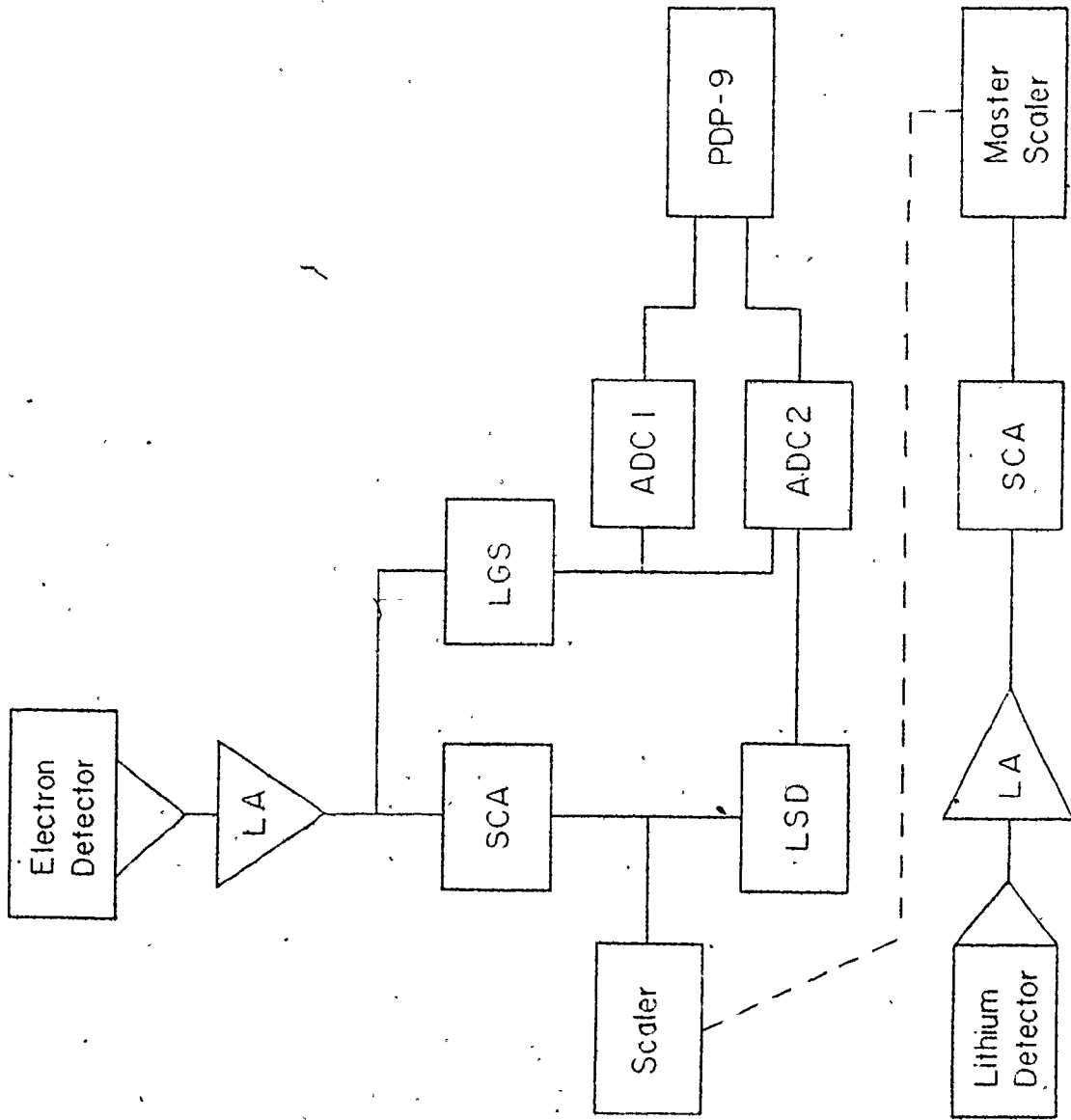
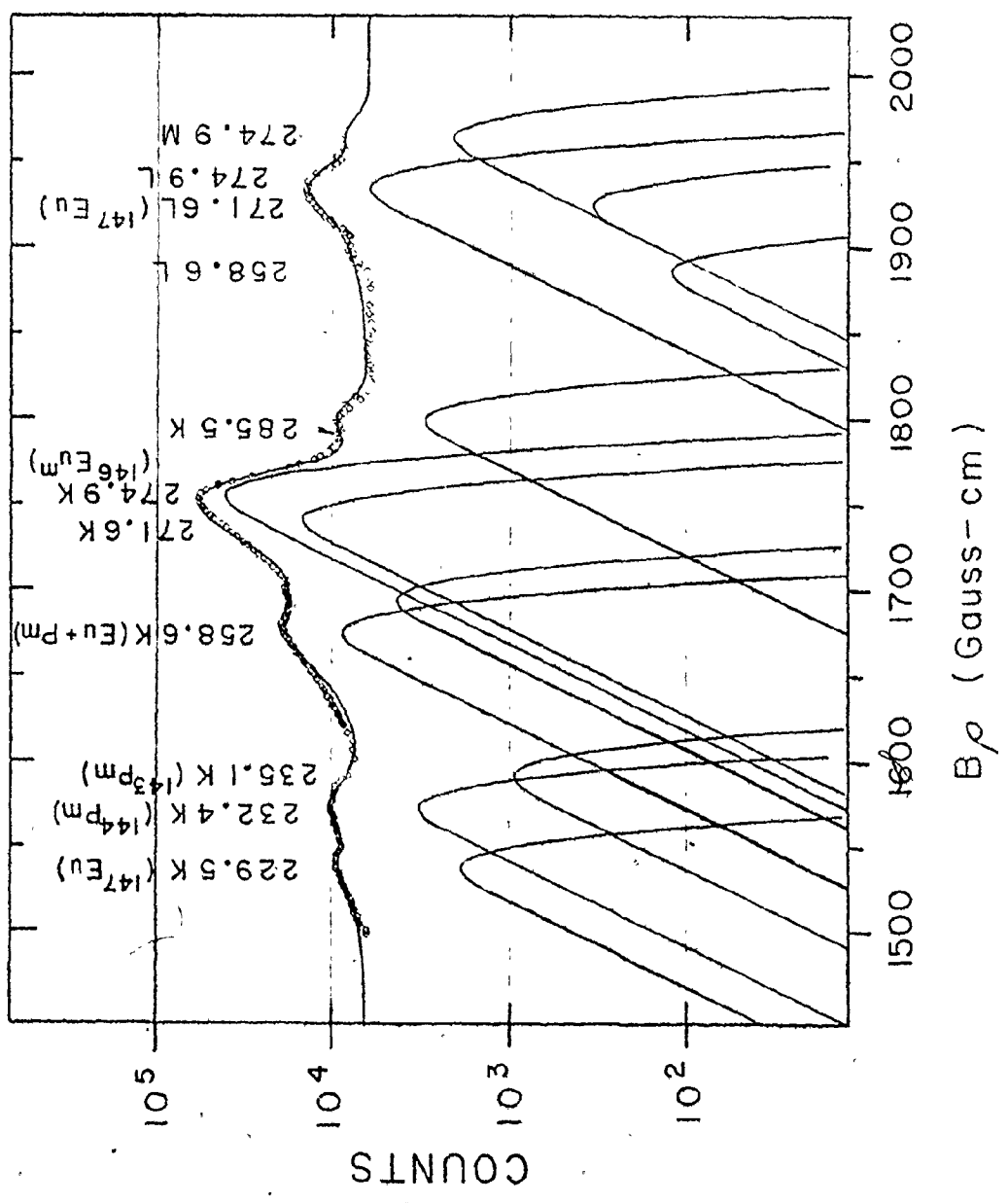


Figure 2.10

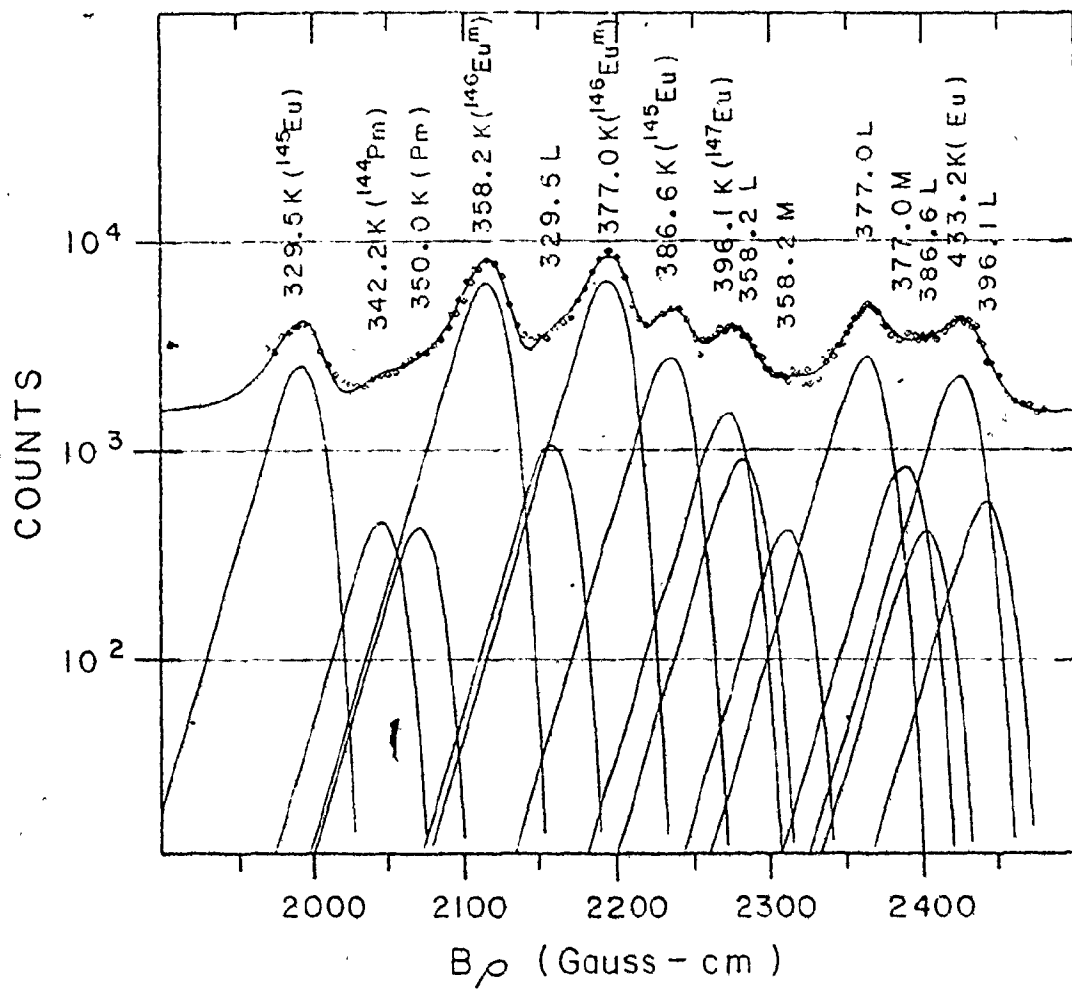
In-beam conversion electron spectrum for 33 MeV Li ions and a ^{142}Nd target. Each point from 1500 to 1990 gauss-cm was collected for the time it took to accumulate 100,000 elastically scattered ^7Li ions in the particle detector. The points from 1990 to 2500 gauss-cm were collected for the time it took to accumulate 40,000 ^7Li counts. The average current was 25 nA.

- (a) The spectrum from 1500-1975 Bp.
- (b) The spectrum from 1975-2500 Bp.



(a)

(b)



CHAPTER 3

GAMMA RAY MEASUREMENTS

(3.1) Energy Measurement and Efficiency Calibration

To establish a level scheme it is usually necessary to obtain accurate values for the energies and intensities of the gamma ray transitions. The energies are determined using standard radioactive sources, for which the transition energies are well known. The pulse heights for the peaks being studied can then be compared with those for the known peaks in the spectrum to determine the unknown energies.

The relative intensity of a given transition, as measured by a detector, will differ from the "true" relative intensity by an amount which is related to the photo-peak efficiency of the detector. In order to determine the photo-peak efficiency a radioactive source with several prominent transitions spread across the energy region of interest, whose relative intensities are known, is required.

A $^{152,154}\text{Eu}$ radioactive source was used both to calibrate the energy, and determine the photo-peak efficiency curves of the 10 cc and 37 cc Ge(Li) detectors used in the present study. The relative intensities, and the energies of the gamma rays emitted by the $^{152,154}\text{Eu}$ source were taken to be those reported by Riedinger et al. (1970) and Barrette et al. (1971). Reaction and radioactive source spectra were taken

with the detectors at 90° to the beam. The efficiency curve of each detector was determined from a spectrum containing only the $^{152,154}\text{Eu}$ source transitions. Strong transitions of interest were then measured against the transitions from the $^{152,154}\text{Eu}$ source by simultaneously recording a spectrum from this radioactive source and the $(^7\text{Li}, 3n)$ reaction both for the in-beam and pulsed beam cases. Having thereby established the energy of these strong lines one could then use them as internal standards when the in-beam and pulsed beam spectra were recorded alone.

3.2 Excitation Functions

The yield of $(^7\text{Li}, xn)$ reaction is a well defined function of the bombarding energy for each value of x . The excitation function increases sharply from zero to some maximum value, and then decreases slowly, as the projectile energy is increased. Moreover, the threshold energy, and the energy for maximum yield depend strongly on the Q -value of the reaction and the size of the Coulomb barrier. In general, the higher the value of x , the higher are the threshold energy, and the energy of maximum yield. It is therefore possible to obtain a good indication to which nucleus a gamma ray belongs, from a measurement of its excitation function. Also, by studying the yield of different $(^7\text{Li}, xn)$ reactions it is possible to choose a bombarding energy which will result in a greater yield for one particular reaction than for the competing

reactions.

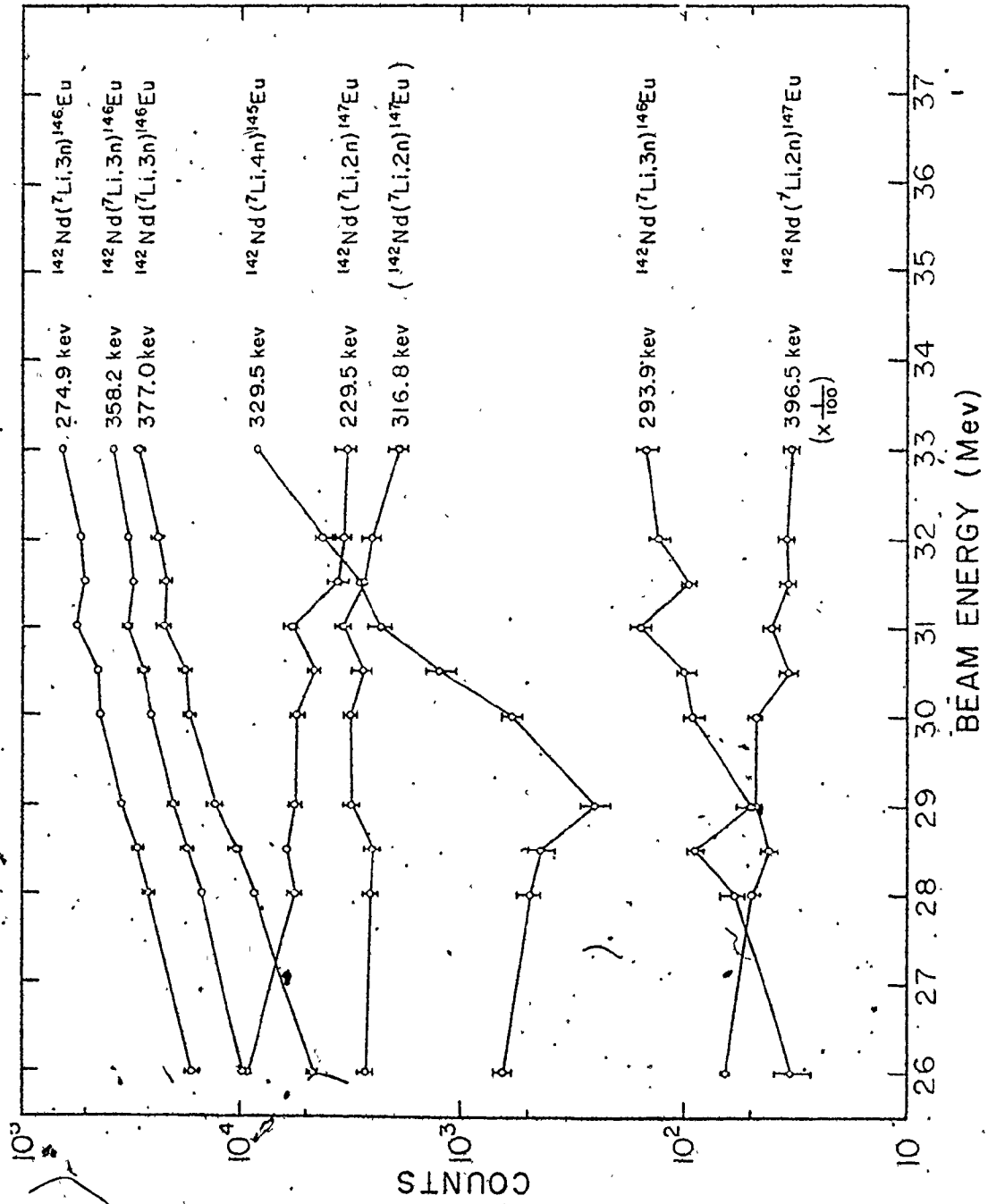
Excitation functions of gamma rays emitted by nuclei formed from $^{142}\text{Nd}(^7\text{Li}, xn)$ reactions were measured so that a bombarding energy could be chosen which would maximize the yield for the $(^7\text{Li}, 3n)$ reaction.

The following set-up was used for this, and all subsequent in-beam and pulsed beam gamma ray measurements. The thin ^{142}Nd target was mounted on a lead frame. It was then placed, 45° to the beam, in a thin walled plastic target chamber on the "0°" beam line. A 10 cc and a 37 cc Ge(Li) detector were placed, opposite each other, 90° to the beam and approximately 6 cm from the target. Gamma ray spectra were collected using a PDP-9 computer with spectra used for the excitation measurements being collected at incident beam energies of 26.0 to 33.0 Mev. The integrated beam current was collected by a Ta beam stop beyond the target.

Gamma ray intensities were extracted at each bombardment energy, using the program SOFT on a PDP-15 computer. These intensities were normalized using the integrated beam current, corrected for detector efficiency, and plotted against the incident beam energy. The resulting excitation functions for some selected gamma rays are shown in Figure 3.1. The excitation function of the 329.5 keV line is affected by the presence of a strong 328 keV line at low bombarding energies. It is also apparent that the yield of the 3n reaction would be greatest at some energy above 33 Mev. However, it was decided

Figure 3.1

Excitation functions for selected gamma rays. The data were normalized by the integrated beam current measured during each run, and have been corrected for the relative detector efficiency. The data points have been joined to aid the eye only.



that an optimum energy would be 33 Mev, as the accelerator is much more stable when operating with 8.25 Mv on the terminal than with higher terminal voltages.

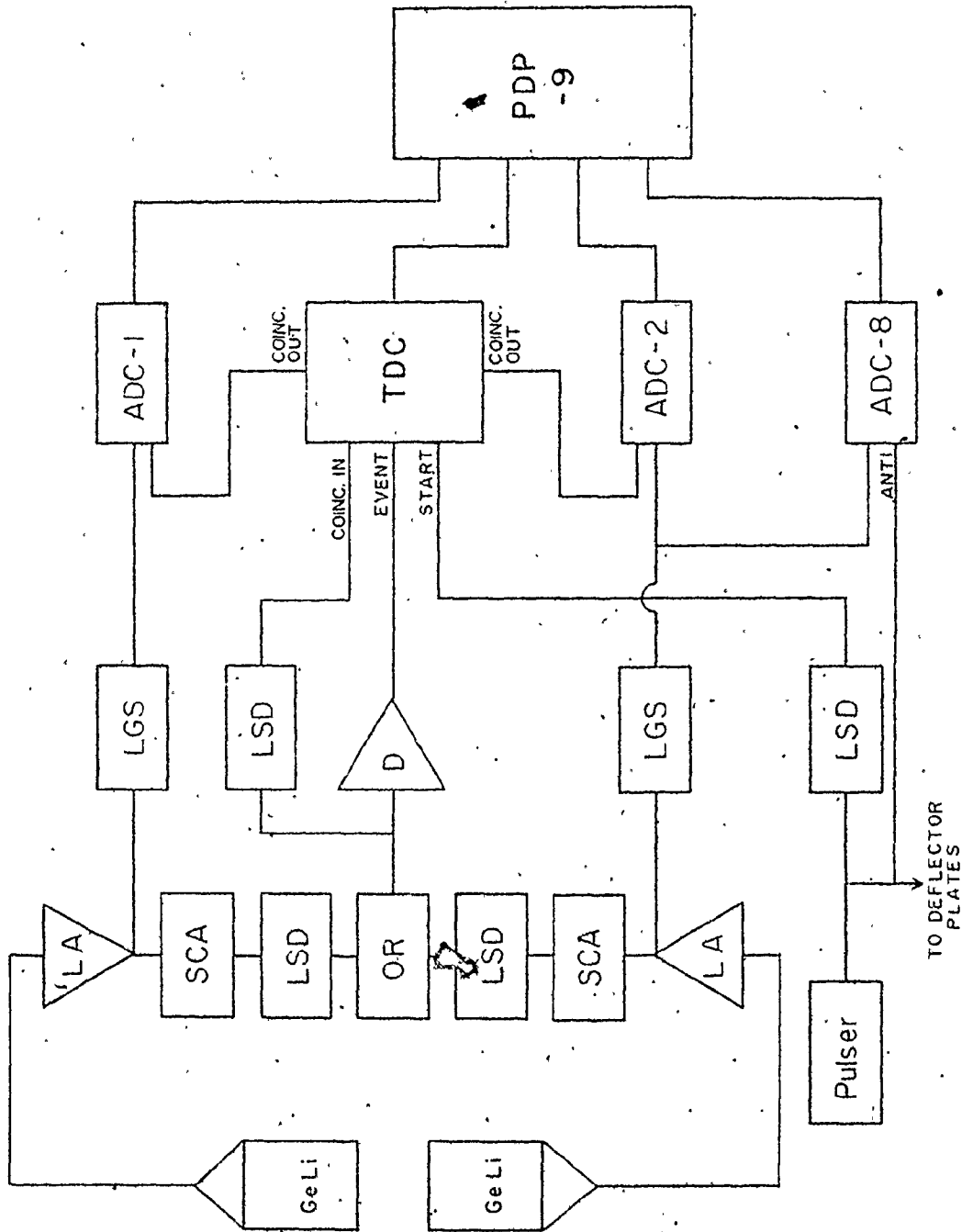
3.3 Pulsed Beam Gamma Ray Measurements

A pulsed beam of ${}^7\text{Li}$ ions was obtained using the pulsing system described in section 2.2(iii)(a) with the deflected beam being stopped from reaching the target by a tantalum aperture placed at the focus in the 0° scattering chamber which is some 20 feet upstream from the target. The beam-off time was arranged to be 0.5 ms, with a beam-on time of 0.5 ms.

The electronic set-up used in the pulsed beam measurements is shown schematically in Figure 3.2. The ADC's marked "1" and "2" in this drawing were operated in the coincidence mode. In this mode, they could only accept an event signal when a gate signal from the coincidence out of the TDC was received. Since the TDC would only accept event signals when the beam was pulsed-off, therefore a coincidence out signal would only be sent during beam-off time periods. Hence, these ADC's accumulated spectra during beam-off time periods. The TDC was given a channel width of 0.4 μs , and thus a live time of 400 μs , for these measurements. The signal from the pulser was also used as a gate signal for ADC 8. Since this ADC was operated in the anticoincidence mode, it therefore accumulated an in-beam spectrum.

Figure 3.2

The electronic circuit used for the pulsed beam gamma ray measurements. The symbols are the same as those used in Figure 2.3.



A spectrum showing both the pulsed beam gamma rays, and those from the $^{152,154}\text{Eu}$ source, is shown in Figure 3.3. The gamma ray intensities required for the pulsed beam internal conversion coefficient calculations were taken from this spectrum. They were extracted with the use of the program SOFT and a PDP-15 computer, and corrected for photo-peak efficiency. A spectrum showing only the pulsed beam reaction gamma rays is shown in Figure 3.4. Little effort was made to identify the origin of the extraneous gamma-rays in the spectrum. However, a spectrum was recorded of the decay of the target after the beam was turned completely off. This identifies at least some of the gamma rays appearing in the pulsed beam spectra which are not coming from the decay of $^{146}\text{Eu}^m$. No lines pertinent to $^{146}\text{Eu}^m$ appear above 450 keV, and so this region is not shown in the gamma ray spectra.

3.4 In-beam Gamma Ray Measurements

The electronic set-up used for the in-beam gamma ray measurements is shown schematically in Figure 3.5, and needs no explanation.

Figure 3.6 shows an in-beam reaction spectrum. The gamma ray intensities required for the in-beam internal conversion calculations were measured from this spectrum.

Having discussed the way in which the data was collected, and analysed, one can now present the results of this investigation.

Figure 3.3

Pulsed beam gamma ray spectrum with $^{152,154}\text{Eu}$ calibrating source for 33 MeV Li ions and a ^{142}Nd target. The spectrum was collected for 1/2 hour at an average pulsed beam current of 0.7 nA. "S" indicates a $^{152,154}\text{Eu}$ source line. (More precise energies can be found in Barrette et al (1971) and Riedinger et al (1970)).

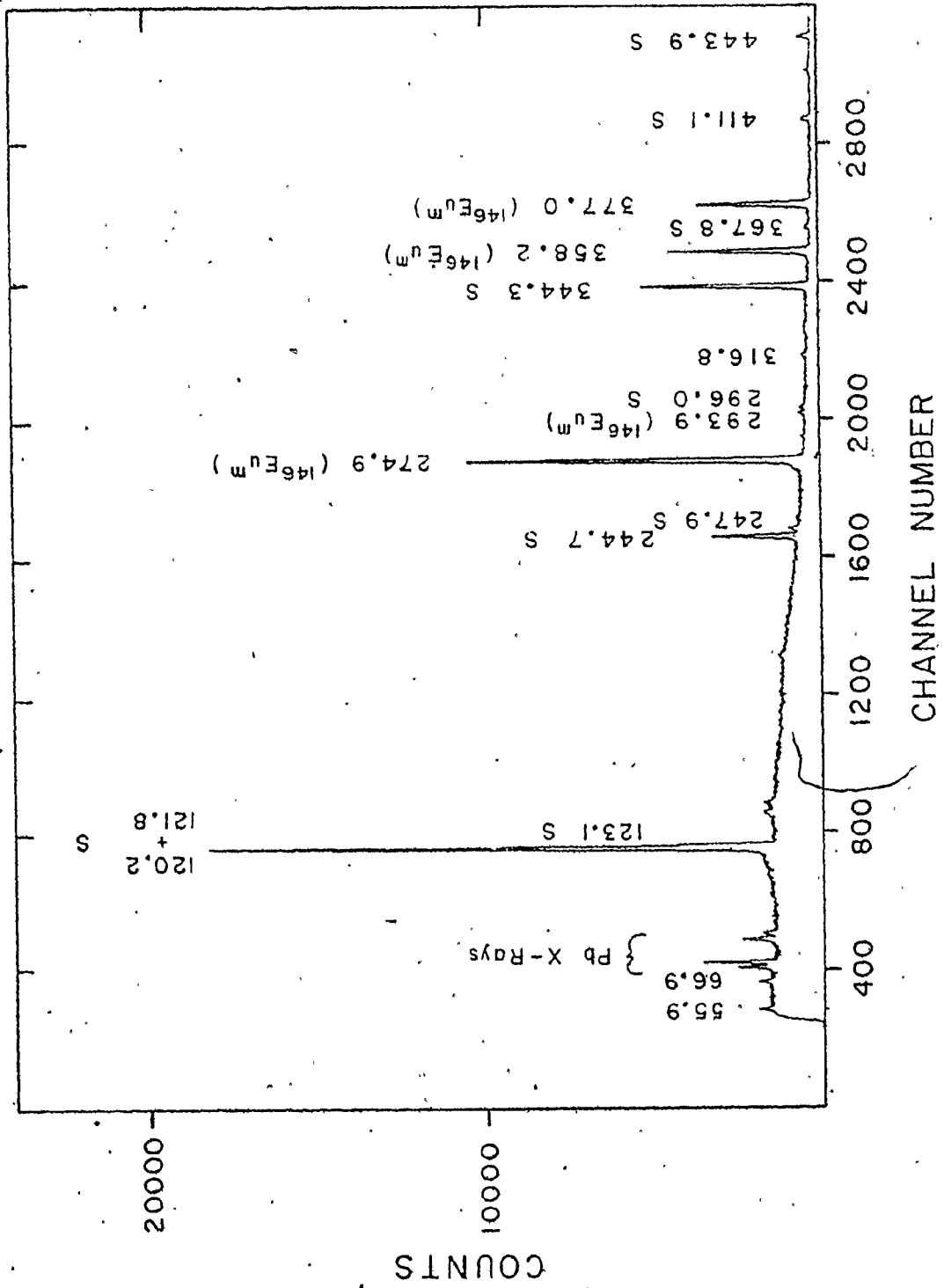




Figure 3.4

Pulsed beam gamma ray spectrum for 32.5 Li ions and a ^{142}Nd target. The spectrum was collected for 1 hour at an average pulsed beam current of 0.3 nA.

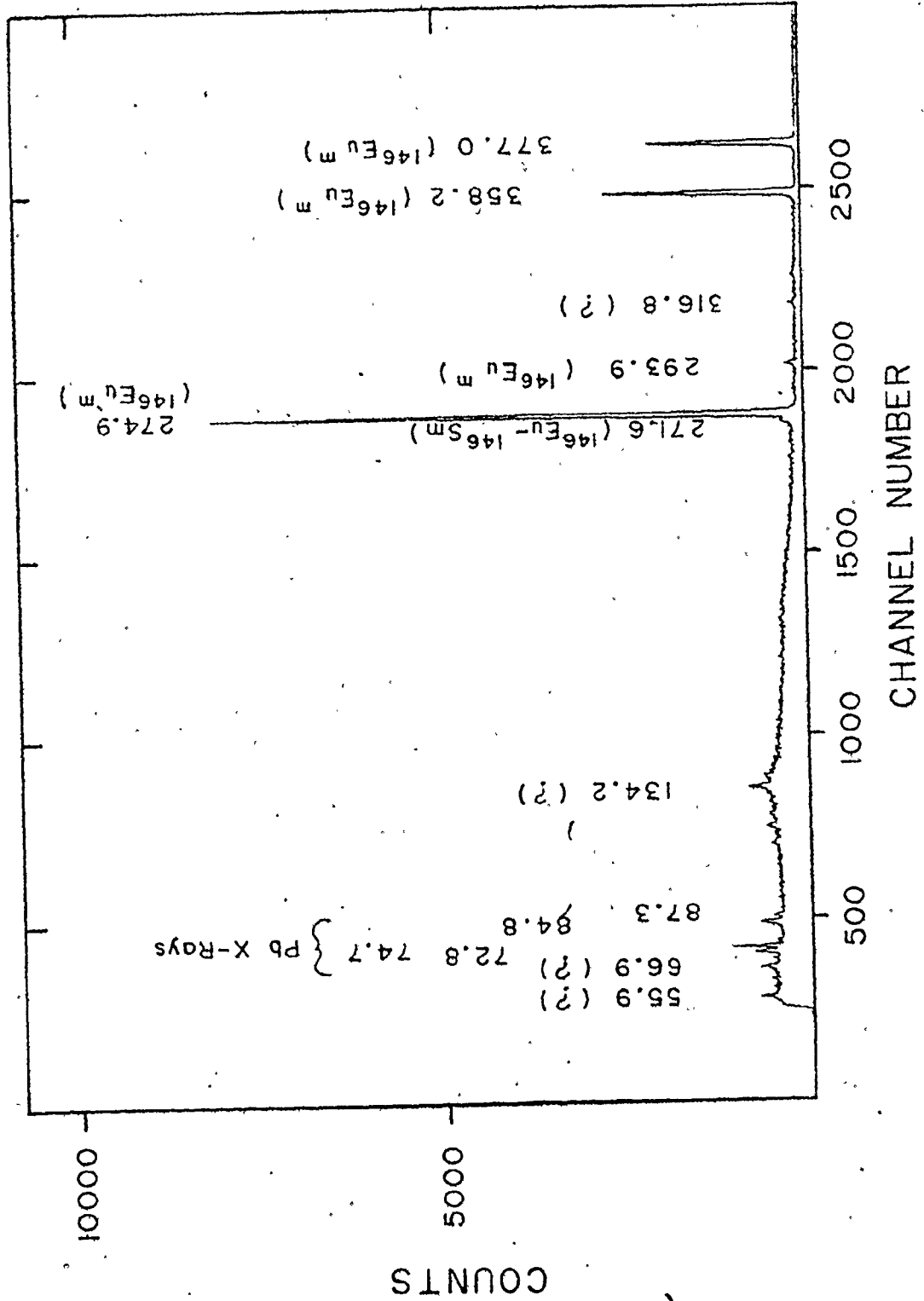


Figure 3.5

The electronic circuit used for the in-beam gamma ray measurements. The symbols are the same as those used in Figure 2.3.

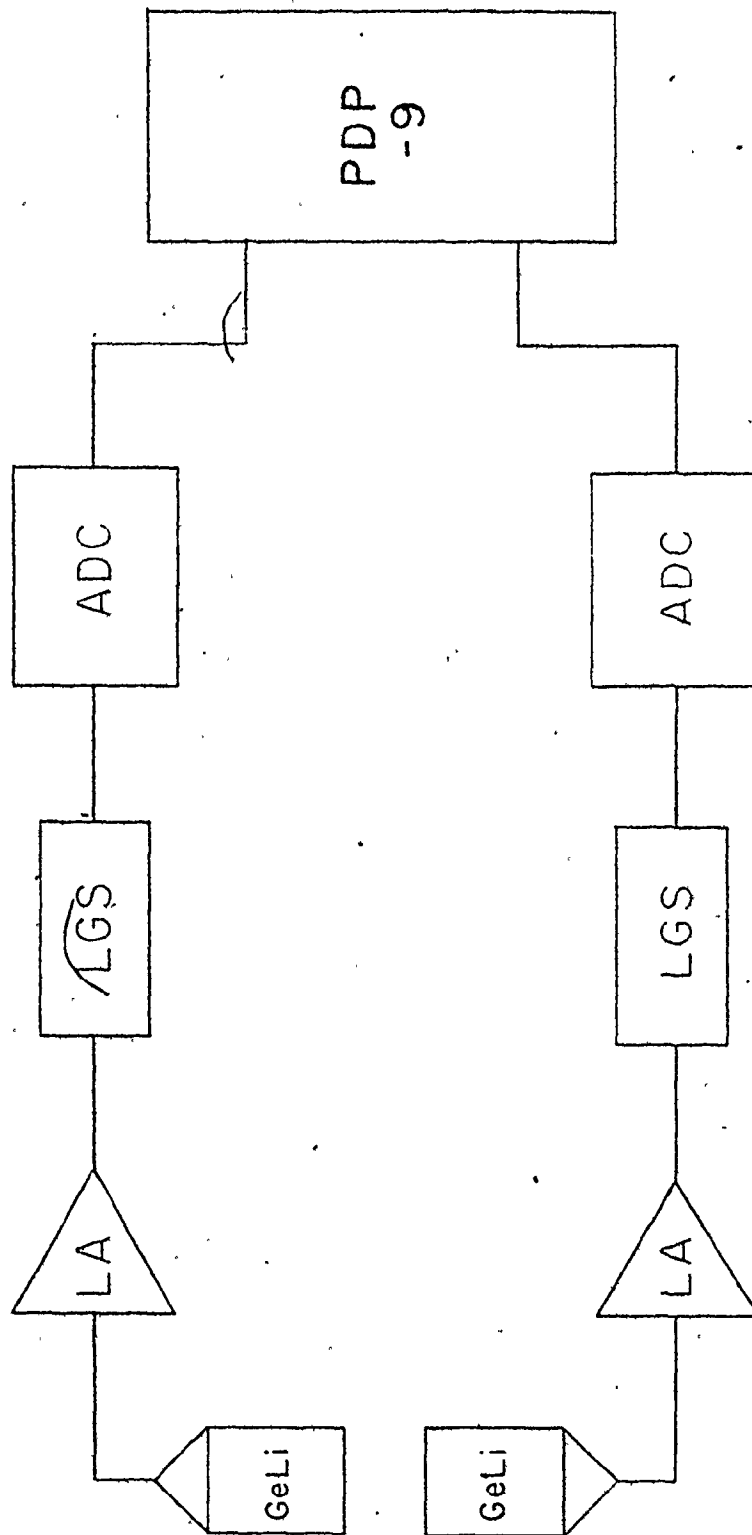
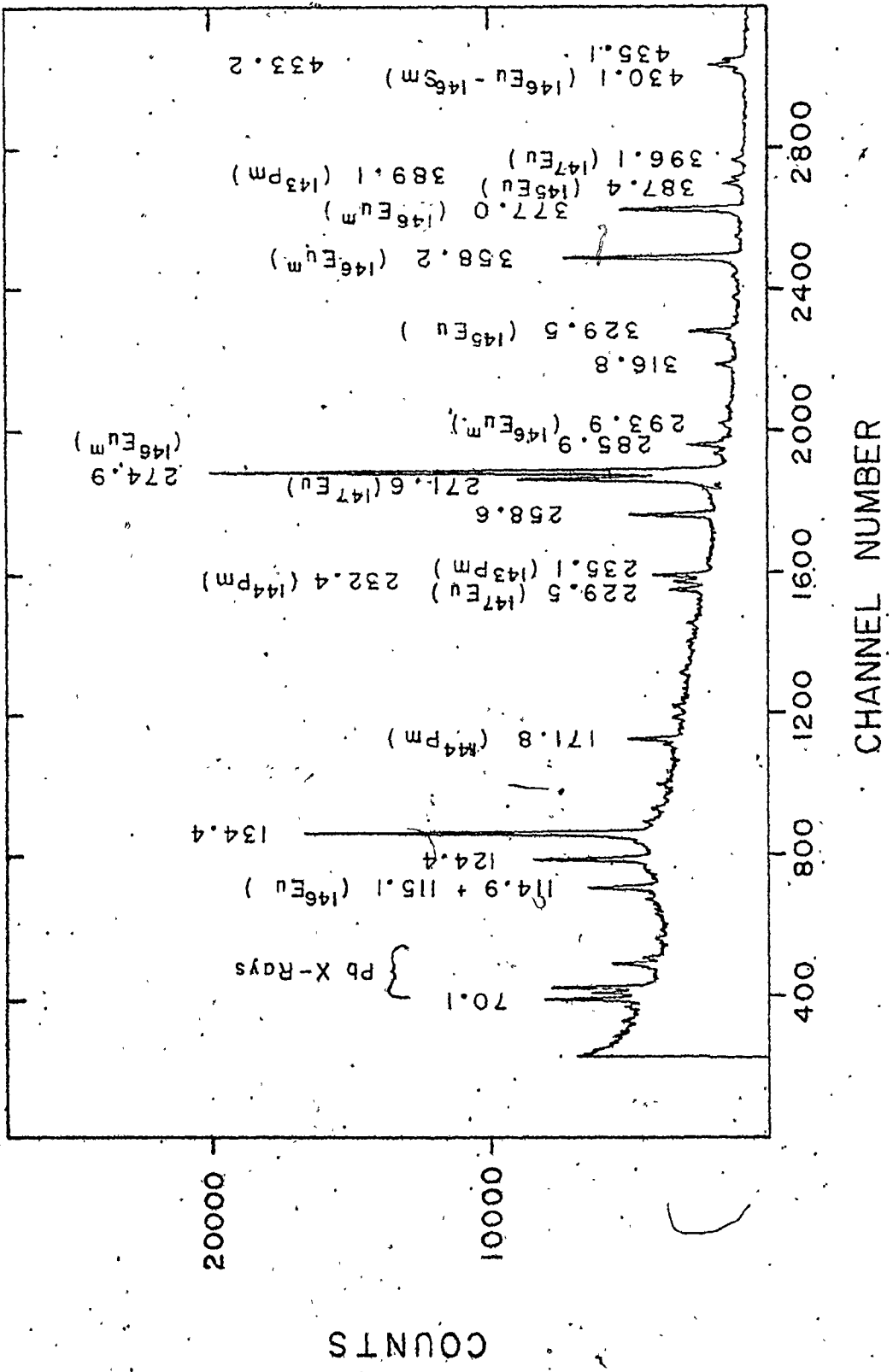




Figure 3.6

In-beam gamma ray spectrum for 33 Mev Li ions and a ^{142}Nd target. The spectrum was collected for 1 1/2 hours at an average current of 0.5 nA.



CHAPTER 4

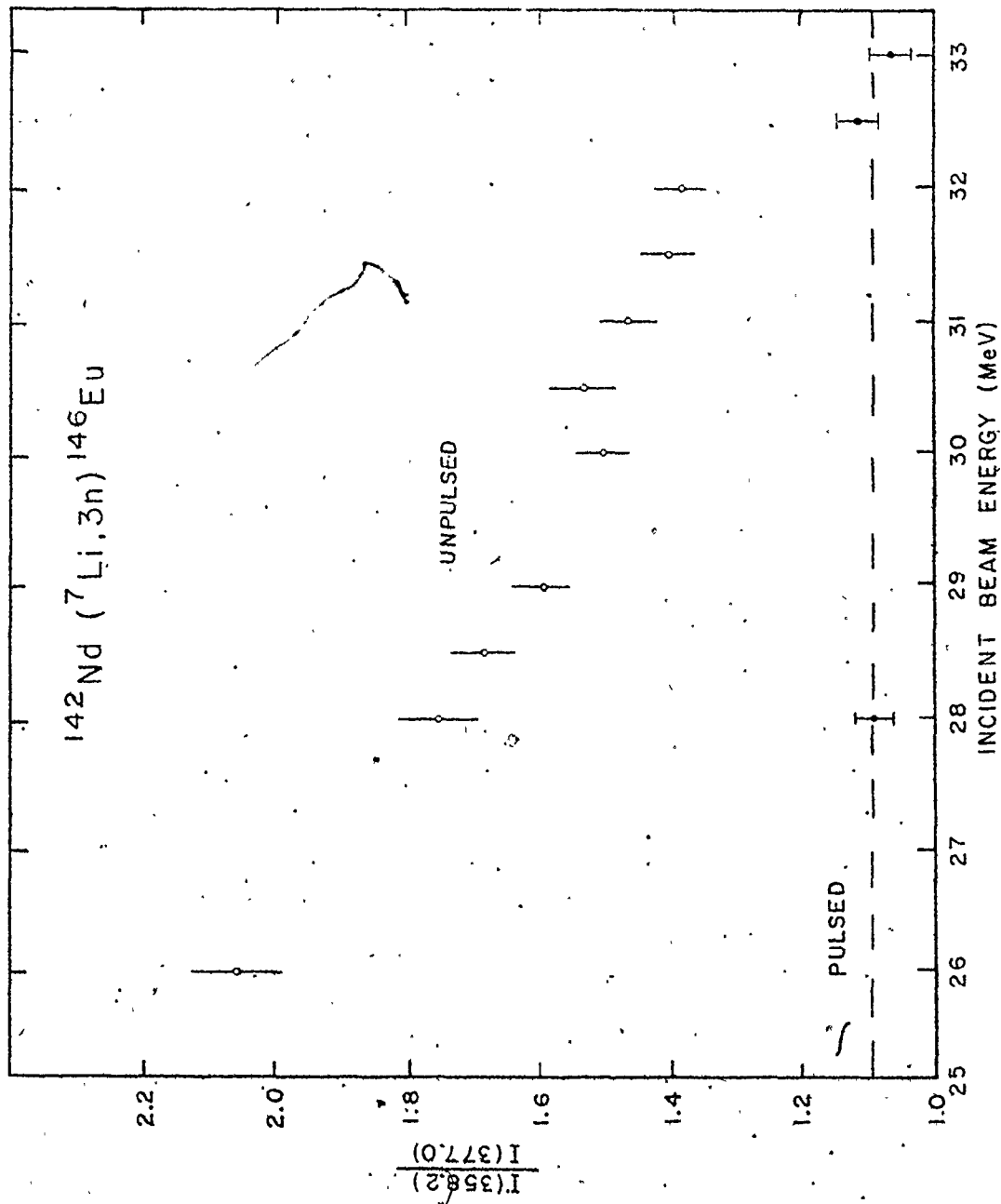
EXPERIMENTAL RESULTS AND DISCUSSION

4.1 Gamma Ray Measurements

Pulsed beam (Figure 3.3), and excitation function measurements (Figure 3.1) identify the 274.9, 293.9, 358.2 and 377.0 keV gamma rays as resulting from the decay of $^{146}\text{Eu}^m$. The relative intensities of these gamma rays, normalized to 100 for the 274.9 keV gamma ray, are shown in table 4.2. These results are consistent with those reported by Gavriilyuk et al. (1973), and Hagemann et al. (1971). It was suggested by these investigators that the 358.2 and 377.0 keV transitions share the same initial state, as shown in Figure 1.1. However, the ratio of the in-beam intensities of the 358.2 and 377.0 keV gamma rays changes with the ^7Li bombardment energy, as Figure 4.1 shows. This result suggests that either the two gamma rays do not share the same initial state or the 358.2 keV line is a doublet with the second member not necessarily a part of the isomer decay. In the interests of simplicity, one looks for a decay scheme for the isomer which satisfies the first alternative.

Figure 4.1

Variation of the ratio of the in-beam intensities of
the 358.2 and 377.0 keV gamma rays with beam energy.



4.2. Conversion Coefficient Measurements

The results of the in-beam, and pulsed beam determinations of the conversion coefficients of the 274.9, 293.9, 358.2 and 377.0 keV transitions are shown in tables 4.1 and 4.2 respectively. As a result of these measurements, the 293.9 and 377.0 keV transitions have been assigned E3 multipolarities. The 274.9 and 358.2 keV transitions are consistent with being pure M1 multipolarity, but the errors in the measurements would permit E2 admixtures of 10 and 50% respectively. These multipolarity assignments, and the total transition intensities are summarized in table 4.3.

The previously proposed decay scheme of $^{146}\text{Eu}^m$, shown in Figure 1.1, assumes M1 or E2 multipolarities for the 274.9, 293.9, 358.2 and 377.0 keV transitions. In view of the discovery that the 377.0 and 293.9 keV transitions are E3 transitions, it is obvious that a new decay scheme is necessary. The new decay scheme will be based on the results shown in table 4.3, and the predictions of the shell model for ^{146}Eu .

4.3 Development of a Decay Scheme for $^{146}\text{Eu}^m$

The ^{146}Eu nucleus has one neutron outside the $N=82$ major shell, and one proton hole in the $Z=64$ shell. The ground state configuration is therefore presumably $\pi 2d_{5/2}^{-1} \nu 2f_{7/2}^1$. The low-lying excited states of ^{146}Eu should be explainable in terms of the $\pi 2d_{5/2}^{-1} \nu 2f_{7/2}^1$, and $\pi 1g_{7/2}^{-1} \nu 2f_{7/2}^1$ multiplets since the excitation of the neutron to the next available orbital, $3p_{3/2}$, requires several hundred keV. The lowest states

Table 4.1 Results of the In-Beam Conversion Coefficient Measurements

Energy (keV)	** THEORETICAL CONVERSION COEFFICIENTS										MULTIPOLARITY
	$\alpha_k(\text{exp}) \times 10^3$	$\alpha_L(\text{exp}) \times 10^3$	$\alpha_k(M1) \times 10^3$	$\alpha_L(M1) \times 10^3$	$\alpha_k(M2) \times 10^3$	$\alpha_L(M2) \times 10^3$	$\alpha_k(E2) \times 10^3$	$\alpha_L(E2) \times 10^3$	$\alpha_k(E3) \times 10^3$	$\alpha_L(E3) \times 10^3$	
*229.5(2)	145(10)	-	155	22	710	140	96	28	340	291	M1 + E2
274.9(1)	107(16)	16(3)	95	13	400	74	56	14	190	120	M1 + < 10% E2
358.2(1)	44(7)	6(1)	47	7	175	30	27	6	78	35	M1 + < 50% E2
377.0(1)	62(9)	24(4)	41	6	145	25	23	5	65	27	E3
*396.1(2)	119(7)	-	36	5	127	20	20	4	54	22	M2

*Transitions in ^{147}Eu used as calibrants. $\alpha_k(\text{exp})$ taken from Grigorev et al (1977).

**Theoretical values interpolated from values listed in Nuclear Data (1968).

Table 4.2 Results of the Pulsed Beam Conversion Coefficient Measurements

Energy (keV)	$\alpha_k(\text{exp}) \times 10^3$	$\alpha_L(\text{exp}) \times 10^3$	** THEORETICAL CONVERSION COEFFICIENTS				$\alpha_L(E3) \times 10^3$	* I_{γ}	MULTIPOLARITY	
			$\alpha_k(M1) \times 10^3$	$\alpha_L(M1) \times 10^3$	$\alpha_k(E2) \times 10^3$	$\alpha_L(E2) \times 10^3$				$\alpha_k(E3) \times 10^3$
274.9(1)***	107(16)	17(3)	95	13	56	14	190	120	100	M1 + < 10% E2
293.9(2)	180(50)	-	78	11	46	11	155	70	1.7(2)	E3
358.2(1)	45(8)	8(2)	47	7	27	6	78	35	52(3)	M1 + < 50% E2
377.0(1)***	62(9)	20(3)	41	6	23	5	65	27	47(3)	E3

* Relative intensities normalized to 100 for the 274.9 keV gamma ray.

** Theoretical values interpolated from values listed in Nuclear Data (1968).

*** Transition used as a calibrant with the $\alpha_k(\text{exp})$ value being taken as that determined from in-beam measurements (Table 4.1).

Table 4.3 Multipolarity Assignments and Total Transition Intensities

ENERGY (keV)	* I	MULTIPOLARITY
274.9 (1)	100	M1/E2
293.9 (2)	1.8 (3)	E3
358.2 (1)	51 (3)	M1/E2
377.0 (1)	46 (3)	E3

* Total transition intensities normalized to 100 for the 274.9 keV transition.

of even parity will arise from the configuration $\pi h_{11/2}^{-1} (lg_{7/2}^{-2} d_{5/2})^{-1} v_{2f_{7/2}}^{-1}$. By interpolating between the experimentally observed excitation energies of one quasiparticle proton states in ^{145}Eu and ^{147}Eu , estimates can be obtained for the excitation energies of similar states in ^{146}Eu (Hagemann et al. (1971)). These estimates are shown in table 4.4. It is interesting to note that zero range calculations for the $\pi h_{11/2}^{-1} (lg_{7/2}^{-2} d_{5/2})^{-1} v_{2f_{7/2}}^{-1}$ configuration predict an ordering of levels with the 2^+ and 9^+ levels being respectively the first, and second lowest excited states in the positive parity group. A metastable situation can therefore exist for the 9^+ state since there will be no state of comparable spin at lower excitation. The 9^+ to 7^- transition would be a relatively low energy M2 transition, and the 9^+ to 6^- transitions would be E3 transitions. Not only would this explain the existence of a 0.230 ms isomer in ^{146}Eu , but, it would also explain how that state could decay with the emission of several gamma rays, as the decay must eventually lead to the 4^- ground state.

A decay scheme has been developed for $^{146}\text{Eu}^m$ using the $(\pi h_{11/2}^{-1} v_{2f_{7/2}}^{-1}) 9^+$ designation of the isomeric state. It is shown in Figure 4.2. The 293.9 and 377.0 keV E3 transitions establish the relative positions of the 9^+ , and the two 6^- levels in the decay scheme. The two 6^- levels could be connected by an 83.1 keV transition, but this would have

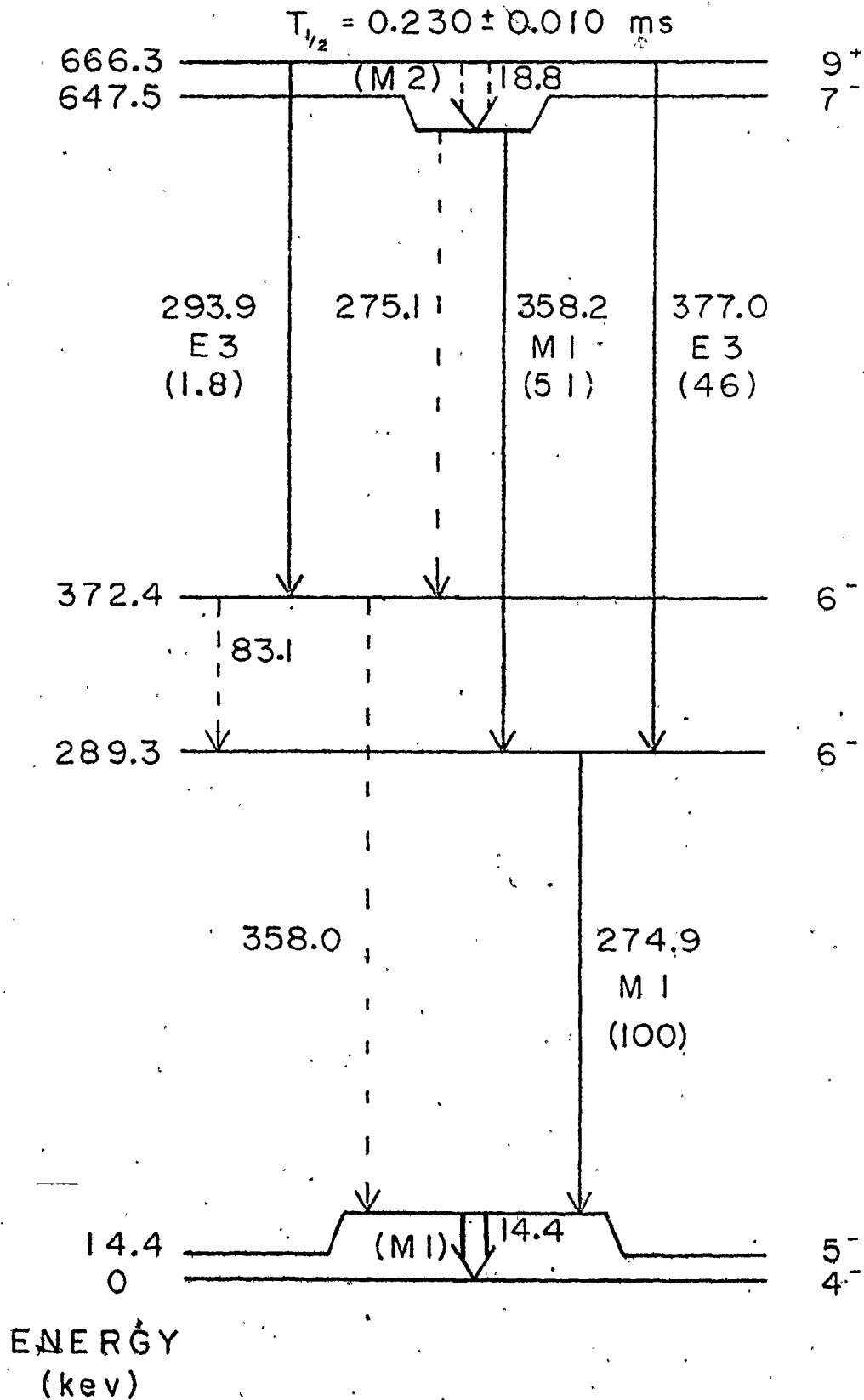
Table 4.4 Estimates of the centroid energies of the $\pi 2d_{5/2}^{-1} \nu 2f_{7/2}^1$, $\pi 1g_{7/2}^{-1} \nu 2f_{7/2}^1$ and $\pi 1h_{11/2}^1 (1g_{7/2}^{-1} 2d_{5/2}^{-2}) \nu 2f_{7/2}^1$ multiplets

ENERGY (kev)	CONFIGURATION	SPIN
0	$\pi 2d_{5/2}^{-1} \nu 2f_{7/2}^1$	$1^-, 2^-, \dots, 6^-$
280	$\pi 1g_{7/2}^{-1} \nu 2f_{7/2}^1$	$0^-, 1^-, \dots, 7^-$
670	$\pi 1h_{11/2}^1 (1g_{7/2}^{-1} 2d_{5/2}^{-2}) \nu 2f_{7/2}^1$	$2^+, 3^+, \dots, 9^+$

(Calculations after Hagemann et al. (1971))

Figure 4.2

The proposed decay scheme of the 0.230 ms isomer in ^{146}Eu . The intensities shown are total transition intensities normalized to 100 for the 274.9 keV transition. The dotted 358.2 and 275.1 keV transitions are included as possibilities only. --- denotes unseen transitions.



been masked by the 84.8 keV Pb x-ray in this investigation.

It is known from Summers-Gill and Islam (1973) that the 358.2 and 377.0 keV gamma rays are both in coincidence with the 274.9 keV gamma ray, but not in coincidence with each other. Obviously, the 358.2 and 377.0 keV transitions must feed the still stronger 274.9 keV transition. If the 358.2 keV line terminates on the lower 5^- state, another level is established 18.8 keV below the 9^+ state which must be fed independently from the isomeric state with a very significant intensity. It seems safe to conclude that this is a 7^- state, so that the independent feeding becomes an unseen, highly converted 18.8 keV M2 transition. Any lower multipolarity (E1, M1, E2) would destroy the isomer's 230 μ s lifetime, and any higher multipolarity would never take an $\sim 50\%$ share of the decay. This assignment is further supported by the fact that the 358.2 keV transition has, at least, a substantial M1 component.

Obviously, the decay from the lower 6^- state to the 4^- ground state can not be accomplished through only the 274.9 keV transition which is known to be nearly pure M1. Intensity considerations rule out the possibility of this being accomplished through a cascade of two 274.9 keV transitions. The existence of an M1 transition whose energy is less than 50 keV, hence not detected in the gamma ray studies of this investigation, is therefore indicated. It seems

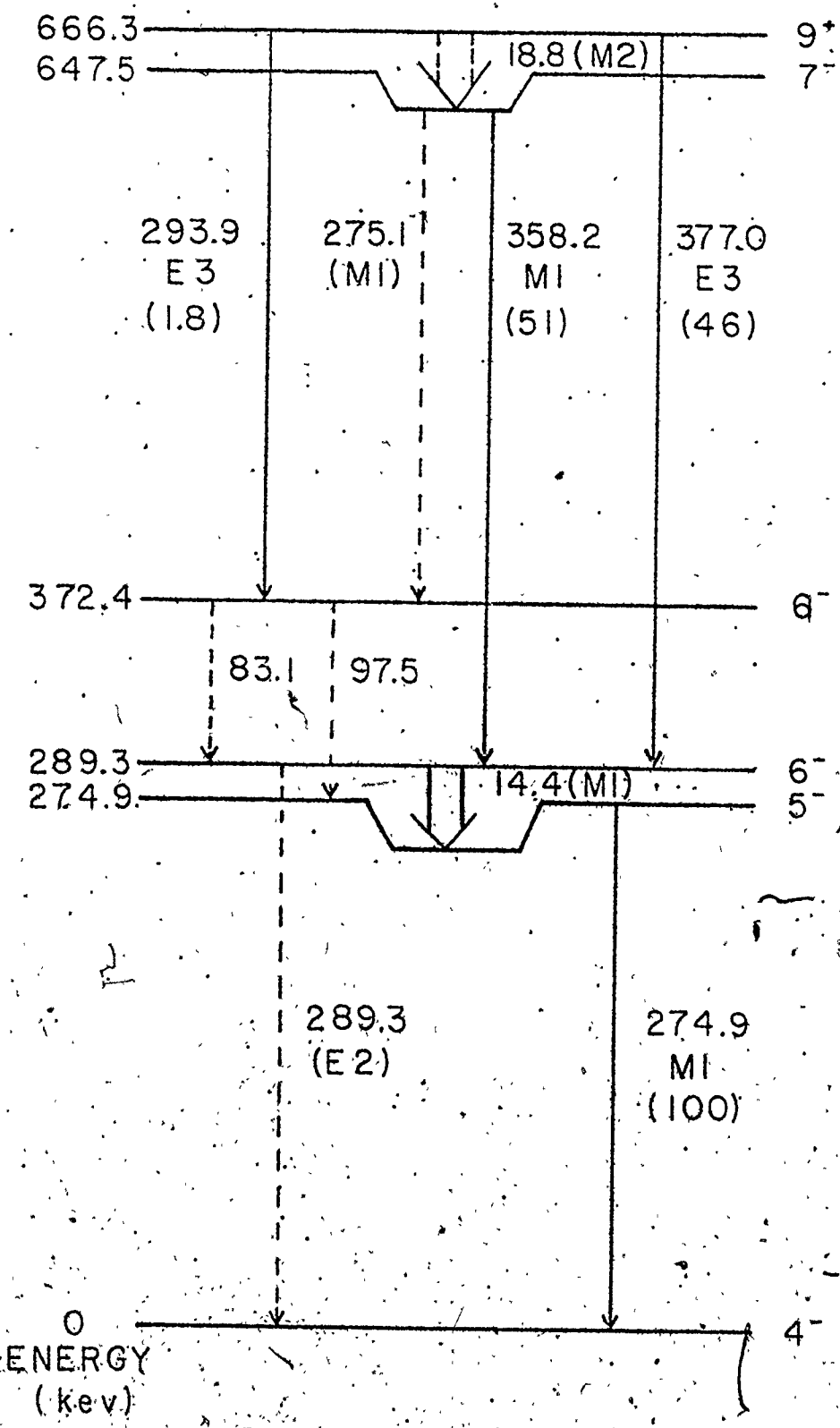
logical to identify this as the 14.4 keV line seen by Summers-Gill and Wender (1975). The lower 6^- state would therefore decay to the ground state through a 14.4/274.9 keV cascade, or a 274.9/14.4 keV cascade. The former situation is illustrated in Figure 4.3, and the latter in Figure 4.2. In either event, the absolute positions of the upper levels are fixed, establishing the isomeric state at an excitation of 666.3 keV. These schemes also raise the possibility of one or both of the 274.9 and 358.2 keV lines being doublets.

No evidence was found in this investigation that forces one choice or the other. There are, however, qualitative grounds for preferring the scheme with the 14.4 keV transition at the bottom. In the former scheme, the upper 6^- level would be expected to decay to the 5^- level by a 97.5 keV transition, which was not observed in this study. As well, a 289.3 keV E2 transition is a more likely method of de-excitation from the lower 6^- level than a 14.4 keV M1 transition. The 274.9 keV transition, which is known to be the strongest transition in the decay, is, however, fed primarily by the 14.4 keV transition in this scheme. In support of the latter scheme, a 5^- state is very likely at low excitation in view of shell model, and empirical evidence from ^{144}Pm , where it is the ground state, and from ^{142}Pr , where it is the first excited state at an excitation energy of 3.7 keV.

Figure 4.3

A decay scheme for $^{146}\text{Eu}^m$ using an alternative placement of the 14.4 keV transition. The intensities shown are total transition intensities normalized to 100 for the 274.9 keV transition. --- denotes unseen transitions.

$$T_{1/2} = 0.230 = 0.010 \text{ ms}$$



0
ENERGY
(keV)

The decay schemes shown in Figures 4.2 and 4.3 propose that the 358.2 keV transition terminates on the lower 6^- level. There is also the possibility that the 358.2 keV transition does not terminate on the lower 6^- level, but, rather on another state somewhat above it. If that state then decayed to the lower 6^- level by an unobserved transition, the coincidence condition of the 358.2 and 274.9 keV transition would still hold. This could be incorporated into a scheme employing either the 14.4/274.9, or the 274.9/14.4 keV cascade from the lower 6^- state to the 4^- ground state. Of course, the unobserved M2 transition at the top of the scheme would then have an appropriately reduced energy. For reasons discussed earlier, it is expected that the 358.2 keV line terminates on a 6^- level. One would therefore have three 6^- states, which is not to be anticipated from shell model considerations, but which can not be positively ruled out. There are, however, qualitative grounds for not preferring this scheme. Shell model considerations lead one to expect two 6^- states, not three. Also, an E2 transition to the 4^- ground state, or an M1 transition to the 5^- state would be more likely methods of de-excitation from this extra 6^- level rather than a low energy (less than 18.8 keV) M1 transition leading to the lowest 6^- level.

Four possible decay schemes for $^{146}\text{Eu}^m$ have now been discussed. Although no evidence was found in this study that rules out any of these schemes, the scheme shown in Figure 4.2

is preferred on qualitative grounds.

The 14.4 keV 5^- excited state in the preferred decay scheme is presumably a member of the $\pi(d_{5/2})^{-1}\nu(f_{7/2})^1$ ground state multiplet. It is not unexpected that a low lying 5^- member of this multiplet should exist, as a 5^- ground state is predicted for ^{146}Eu on the basis of the Brennan-Bernstein coupling rules (Brennan et al. (1960)). Also, calculations performed by Gavriilyuk et al. (1973) to determine the ordering of the levels of the $\pi(d_{5/2})^{-1}\nu(f_{7/2})^1$ multiplet predict a 4^- ground state with a low-lying 5^- level being the first excited state of the multiplet. The formula developed by Pandya (1956) relating particle-hole and particle-particle interaction energies was used in the calculations, with the interaction energies being taken from a study by Kern et al. (1968) of the $\pi(d_{5/2})^0\nu(f_{7/2})^1$ levels of ^{142}Pr . The results of these calculations are summarized in table 4.5.

The 293.9 keV E3 transition has been found to be retarded by a factor of 3 from the Weisskopf estimate of its transition rate, while the 377.0 keV E3 transition is enhanced by a factor of 1.7. This, along with the closeness of the two 6^- levels in the decay scheme, leads one to believe that the two 6^- levels are mixtures of the $\pi 2d_{5/2}^{-1}\nu 2f_{7/2}^1$ and $\pi 1g_{7/2}^{-1}\nu 2f_{7/2}^1$ configurations. The theoretical transition rates were determined from the expressions for the Weisskopf estimates found in Preston (1962).

Table 4.5 Calculated and Observed Spectra for the $\pi(2d_{5/2})^{-1}\nu(2f_{7/2})^1$ Configuration of ^{146}Eu

E_{ex} (CALC.) (kev)	I_{π}	E_{ex} (EXP.) (kev)	I_{π}
0	4 ⁻	0	4 ⁻
38.8	5 ⁻	14.4	5 ⁻
65.5	2 ⁻	115.52**	3 ⁻ *
101.9	6 ⁻	230.19**	2 ⁻ *
142.8	3 ⁻	289.3	6 ⁻
170.5	1 ⁻	384.76**	1 ⁻ *

* Levels not involved in the decay of $^{146}\text{Eu}^m$.

** Energies from Gavriluk et al. (1973).

4.4 The Recent Investigation by Ercan et al.

Ercan et al. (1980) have studied the decay of $^{146}\text{Eu}^m$ using the (p,2n) reaction on ^{147}Sm with 19 to 22 Mev proton beams. Three and four parameter $\gamma\gamma$ -coincidence experiments were performed, and a conversion electron spectrum was measured between the cyclotron beam bursts.

The results of this investigation are supportive of the decay scheme shown in Figure 4.2. The multipolarity assignments, which were based on conversion coefficient measurements, agree with those shown in table 4.3. The 14.4 keV gamma ray was found to be in coincidence with the 274.9, 293.7, 358.2, and 377.0 keV gamma rays. Also, an 83.3 keV gamma ray was found to be in coincidence with the 274.9, and 293.7 keV gamma rays. However, the most interesting feature of their work is the presence of 275-275 keV and 294-358 keV coincidences which prove that both the 358.0 and 275.1 keV dotted transitions of Figure 4.2 actually occur. Also, extremely weak 56.0, and 316.6 keV gamma rays were observed in several coincidence gates. These transitions are not in our decay scheme, shown in Figure 4.2, although delayed gamma rays of 55.9, and 316.8 keV were observed in the $^{142}\text{Nd}(^7\text{Li},3n)$ pulsed beam experiment (Figure 3.4). They were not placed in the decay scheme because no evidence was found to confirm that they were associated with the decay of $^{146}\text{Eu}^m$. They are too weak to permit accurate half-life measurements and the

excitation function of the 316.8 keV gamma ray would seem to indicate that it was formed by the (${}^7\text{Li}, 2n$) reaction, as is shown in Figure 3.1. Indeed, there is a known 318.6 keV gamma ray in the level scheme of ${}^{147}\text{Eu}$.

The decay scheme of ${}^{146}\text{Eu}^m$ proposed by Erçan et al is shown in Figure 4.4. The presence of the extra 5^- state at 316.6 keV distinguishes this decay scheme from that shown in Figure 4.2. It is the weak 56.0-316.6 keV cascade connecting the upper 6^- level and the 4^- ground state which confirms the placement of the 14.4 keV transition at the bottom of the decay scheme.

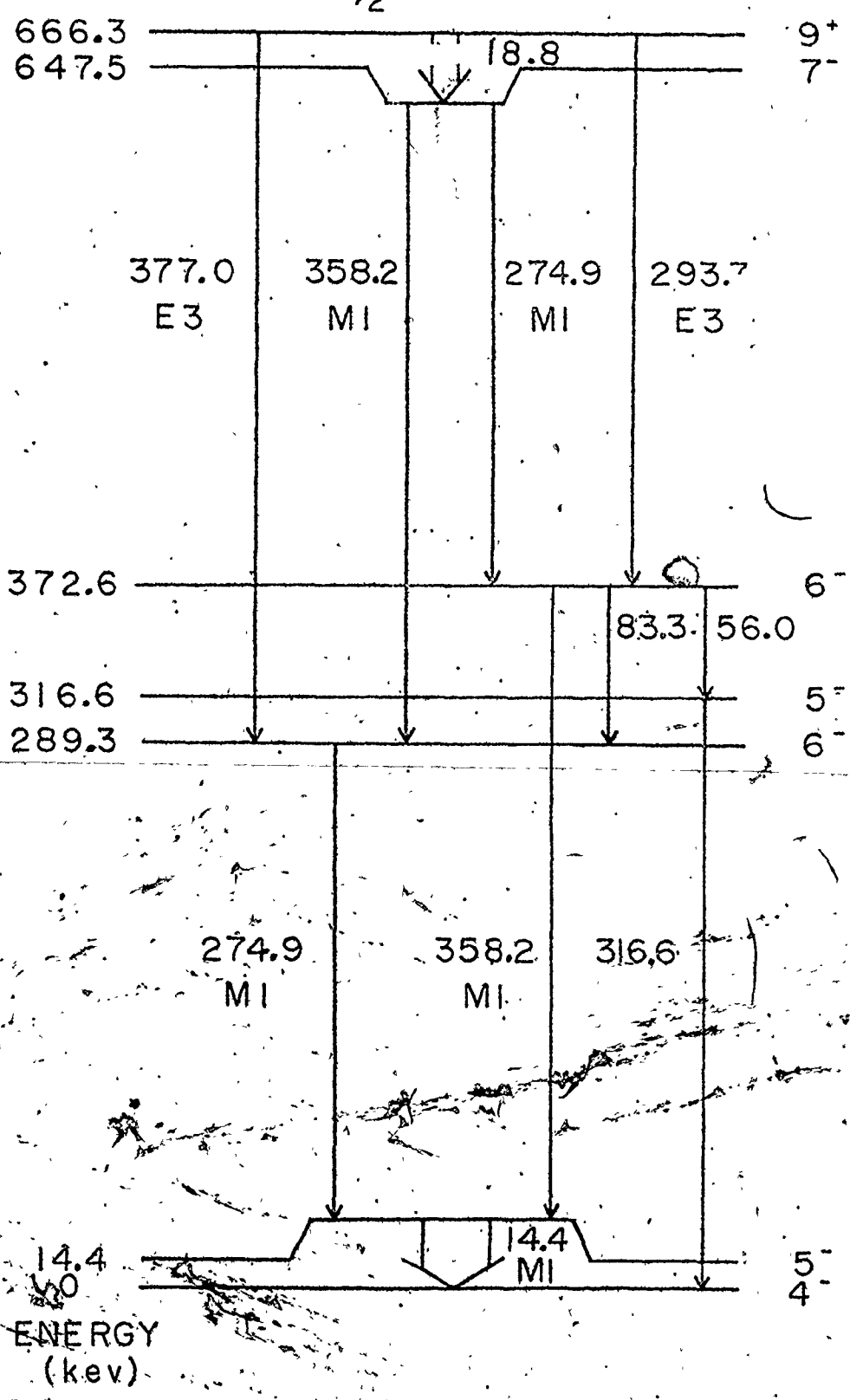
4.5 Conclusions

A decay scheme for ${}^{146}\text{Eu}^m$ has been proposed which is consistent with the results of the present, and all previous, investigations, and which is in agreement with the conclusions of the most recent study. Further $\gamma\gamma$ -coincidence studies should resolve the question of the placement of a 5^- level at an excitation energy of 316.6 keV. A full shell model calculation can now be performed with a comparison to the ${}^{146}\text{Eu}^m$ decay scheme yielding a means of determining empirical values for the matrix elements of the neutron-proton two-body interaction.

Figure 4.4

The decay scheme for $^{146}\text{Eu}^{\text{m}}$ proposed by Ercan et al. (1980). The intensities of the transitions in the decay were not reported.

$$T_{1/2} = 235(25) \mu s$$



ENERGY
(kev)

REFERENCES

- Barrette, J., Barrette, M., Boutard, A., Lamoureux, G., Monaro, S., and Markiza, S. (1971). *Can. Journal of Physics* 49, 2462.
- Brennan, M.H., and Bernstein, A.M. (1960). *Phys. Rev.* 120, 927.
- Ekström, C., Ingelman, S., Olsmats, M., Wannberg, B. (1972). *Phys. Scr.* 6, 181.
- Ercan, A., Broad, R., Piiparinen, M., Nagai, Y. Pengo, R., and Kleinheinz, P. (1980). *Z. Phys. A* 295, 197.
- Gavrilyuk, V.I., Gromov, K. Ya., Klyuchnikov, A.A., Kupryashkin, V.T., Latyshev, G.D., Makovetskii, Yu. V., and Feoktistov, A.I. (1973). *Izv. Akad. Nauk SSSR, Ser. Fiz.* 37, 1839.
- Geiger, J.S. (1965), AECL Report CRGP-1214 (unpublished).
- Grigorev, E.P., Zotoravin, A.V., Kaminov, S.V., Sergeev, V.O., Vylov, T., Kalimnikov, V.G. (1977). *Izv. Akad. Nauk SSSR, Ser. Fiz.* 41, 1203.
- Hagemann, U., Neubert, W., Peker, L.K., Schulze, W., and Stary, F. (1971). *JINR E6*, 6193, Dubna.
- Kern, J., Struble, G.L., Sheline, R.K., Junney, E.T., Koch, H.R., Maier, B.P.K., Gruber, G., and Schult, O.W.B. (1968), *Phys. Rev.* 103, 956.
- Khoo, T.L. (1972). Ph.D. Thesis, McMaster University.
- Nuclear Data* (1968). A4, 14.
- Nuclear Data Sheets* (1974). 12, 229.

Nuclear Data Sheets (1975). 14, 448.

Nuclear Data Sheets (1978). 25, 104.

Pandya, S.P. (1956). Phys. Rev. 103, 956.

Preston, M.A. (1962). "Physics of the Nucleus", Addison-Wesley Co. Inc., Reading Mass.

Rakiyenko, Yu. N., Klyucharev, A.P., Romaniy, I.A., Skakyn, E.A., Yatsenko, G.I. (1968). Ukr. Fiz. J. 13, 478.

Remayev, V.V., Gritsyna, V.T., Klyucharev, A.P. (1962). JETP 42, 408.

Riedinger, L.L., Johnson, N.R., and Hamilton, J.H. (1970) Phys. Rev. C2, 2358.

Summers-Gill, R.G., and Islam, A. (1973). (unpublished).

Summers-Gill, R.G., and Wender, S. (1975). (unpublished).